MSM PHOTODIODE AS THE SWITCHING ELEMENT IN A PHOTOSWITCH-BASED CLASS E MICROWAVE POWER AMPLIFIER

A Thesis
presented to
the Faculty of the Graduate School
at the University of Missouri-Columbia

In Partial Fulfillment
of the Requirement for the Degree

Master of Science

---

by

BRADY SMITH

Dr. Robert O'Connell, Thesis Supervisor

AUGUST 2008

The undersigned, appointed by the dean of the Graduate School, have examined the thesis entitled

MSM PHOTODIODE AS THE SWITCHING ELEMENT IN A PHOTOSWITCH-BASED CLASS E MICROWAVE POWER AMPLIFIER

Presented by Brady Smith,

A candidate for the degree of Master of Science,

And hereby certify that, in their opinion, it is worthy of acceptance.

____

Professor Robert M. O'Connell

____

Professor William C. Nunnally

____

Professor John M. Gahl

ACKNOWLEDGEMENTS

This thesis would not be possible without the help of a few people.

I would like to thank Dr. Robert O'Connell for his aid and guidance during my research. His helpful guidance and interest in the research has saved me countless wasted hours and improved the final result.

I would also like to thank Dr. William Nunnally for his ideas, and for motivating me to work harder and try different approaches.

My thanks are extended to Dr. John Gahl, who is dedicating his time to be on my thesis committee.

I would like to thank Dr. Gregory Triplet, Dr. Jae Kwon, Dr. Mahmoud Almasri, and Lin Li for the use of their facilities and their help attempting to fabricate the device.

Finally, I thank Bryan Pratte, who has helped me greatly in the lab throughout the experimental phase of this work.

TABLE OF CONTENTS

ACKNOWLEDGEMENTS ii

LIST OF FIGURES vi

LIST OF TABLES viii

CHAPTER 1 1

INTRODUCTION 1

1.1 SUMMARY OF CHAPTERS 2

CHAPTER 2 4

THEORETICAL BACKGROUND.. 4

2.1 PHOTODETECTORS.. 4

2.2 LASER DIODE.. 6

2.2.1 Laser Diode Basics.. 6

2.2.2 Fabry-Perot Etalon.. 7

2.2.3 Beam Waist and Optical Confinement.. 8

2.3 RAY MATRICES FOR OPTICAL SYSTEMS.. 9

2.3.1 Ray Matrix for a Distance d.. 9

2.3.2 Ray Matrix for a Thin Lens.. 10

2.4 MICROELECTRONIC FABRICATION.. 11

2.4.1 Photolithography.. 11

2.4.2 Wet vs. Dry Etching of the Semiconductor Substrate.. 12

2.4.3 Metal Deposition.. 13

2.4.4 Liftoff vs. Etching for Metal Patterning.. 14

CHAPTER 3.. 16

PHOTOSWITCH DESIGN.. 16

3.1 BULK VS. LT GaAs 17

3.2 GENERAL PHOTOSWITCH GEOMETRY……………………..…………….. 19

3.3 FINGER WIDTH AND SPACING AND ACTIVE AREA…………..……… 22

3.4 BREAKDOWN VOLTAGE……………………..………………………… 24

3.5 LASER SPOT SIZE……………………………..……………………… 24

3.6 PHOTOSWITCH ANALYSIS AND PERFORMANCE SUMMARY...…….. 27

3.7 PHOTOSWITCH FABRICATION…………………..………………………. 29

CHAPTER 4………………………………………………..……………………… 31

LASER CIRCUIT SETUP……………………………………………..…………….. 31

4.1 WAVELENGTH………………………………………..……………….. 31

4.2 LASER MODULATION………………………………………..……………. 31

4.2.1 Frequency-Doubled System…………………………..…………….... 34

4.2.2 Electrically Modulated System……………………………..………….. 35

4.2.3 Choice of Laser Circuit…………………………..……………….. 36

4.3 LASER MOUNTING………………………………..………………... 37

4.4 BIAS TEE REQUIREMENTS AND LASER DRIVE SIMULATION…..….. 38

4.5 LASER FOCUSING………………………………..……………………… 41

CHAPTER 5…………………………………………………..………………… 45

MICROSTRIP CLASS E AMPLIFIER……………………………..…………….. 45

5.1 CLASS E AMPLIFIERS……………………………………..………….. 45

5.2 LUMPED-ELEMENT DESIGN………………………………..………….. 46

5.3 MICROSTRIP REALIZATION…………………………..…………….. 53

CHAPTER 6…………………………………………..……………………… 58

EXPERIMENTAL SET-UP, RESULTS, AND CONCLUSIONS……..……………. 58

6.1 FIRST EXPERIMENTAL SET-UP……………………………..…………. 58

6.2 FIRST RESULTS…………………………………..………………. 62

6.3 FINAL EXPERIMENTAL SET-UP……………………..………………… 65

6.4 FINAL RESULTS………………………………..……………………… 68

6.5 CONCLUSIONS……………………………………………..…………….. 71

CHAPTER 7……………………………………………………..…………… 73

FUTURE WORK…………………………………………...……………… 73

7.1 OPTICAL MODULATION AND AMPLIFICATION…………..……….….... 73

7.2 PHOTOSWITCH DESIGN……………………..……………………..… 74

7.3 LIGHT COUPLING……………………………………..…………….…. 75

APPENDIX A……………………………………………………..…………..… 77

COMPUTATION OF CHARACTERISTIC IMPEDANCE AND EFFECTIVE DIELECTRIC CONSTANT OF A MICROSTRIP TRANSMISSION LINE..……..... 77

APPENDIX B……………………………………...……………………..… 79

DEVICE PHOTOMASK……………………………………..……………….…. 79

REFERENCES……………………………………...…………………..….. 81

LIST OF FIGURES

Figure Page

Figure 2.1: Comparison of drift length in PIN photodiode and photoconductor..….. 5

Figure 2.2: Diagram for calculating ray matrix for a distance d………………..……. 9

Figure 2.3: (a) Wet etching vs. (b) dry etching……………………………..…...… 12

Figure 2.4: Liftoff…………………………………………………………..…... 14

Figure 2.5: Metal etching……………………………………………..……… 15

Figure 3.1: Photoswitch design in [1]…………………………………….…….. 19

Figure 3.2: MSM photodiode……………………………………………….…….. 20

Figure 3.3: New recessed electrode geometry from [12]……………………..…... 21

Figure 3.4: Finger width, w, and spacing, d. Black represents electrodes…….…….. 22

Figure 3.5: Variables used to calculate maximum light intensity…………..……... 26

Figure 4.1: Mach-Zehnder intensity modulator…………………………..….. 32

Figure 4.2: 1550 nm and 830 nm laser systems………………………………..….. 34

Figure 4.3: Chosen system: electrically modulated 830 nm system……………..….. 36

Figure 4.4: Triangular taper for laser mounting…………………………..…….. 38

Figure 4.5: Bias tee……………………………………………………………...… 38

Figure 4.6: Bias ranges A-B for diode laser, given threshold current of 140 mA on P_{opt} vs. I_f graph (a). (b) is diode I_f vs. V_f curve……………...……... 39

Figure 4.7: PSpice simulation of bias tee drive circuit and laser load………..…... 40

Figure 4.8: Laser focusing reference diagram…………………………..…………. 42

Figure 5.1: Lumped-element class E amplifier…………………………..………… 45

Figure 5.2: Class E switch waveforms [19]……………………………….……….. 46

Figure 5.3: Necessary impedance transformation………………………………... 48

Figure 5.4: First impedance transformation stage……………………………… 49

Figure 5.5: Lumped-element class E amplifier without harmonic suppression……... 49

Figure 5.6: PSpice simulation of class E amplifier without harmonic suppression…. 50

Figure 5.7. PSpice simulation of class E amplifier with harmonic suppression…….. 52

Figure 5.8: Microstrip realization of class E amplifier…………………….... …. 53

Figure 5.9: Microstrip class E amplifier…………………………...………... 56

Figure 6.1: Excitation system………………………………………...……... 58

Figure 6.2: Electrically modulated laser system…………………………….. 61

Figure 6.3: Class E amplifier output……………………………………… 63

Figure 6.4: Altered, final class E amplifier setup……………………………… 64

Figure 6.5: Final laser circuit……………………………………………... 65

Figure 6.6: Optically modulated laser system……………………………….. 66

Figure 6.7: photodiode (A) and filter (B)…………………………………… 67

Figure 6.8: Filter derived from class E amplifier…………………………… 67

Figure 6.9: Final class E amplifier circuit……………………………….... 68

Figure 6.10: Input voltage, V_{in}……………………………………...…….. 69

Figure 6.11: Output voltage, V_{out}…………………………………...…….. 69

LIST OF TABLES

Table | Page

Table 3.1: Comparison of photoswitch in [1] with the adopted MSM photodiode…… 22

Table 3.2: Summary of parameters for the designed photoswitch…………………….. 29

Table 4.1: Minimum specifications for bias tee……………………………………….. 39

CHAPTER 1

INTRODUCTION

The purpose of this study is to develop and characterize a radio frequency class E amplifier with an optical device as the switching element. The target use of this type of amplifier is as the final-stage power amplifier in the transmit-receive module of a phased-array radar system. The goal of the photonic design is to improve efficiency and so also reduce heat removal requirements, reducing the size, weight, and power requirements of the radar system. Optical switching is capable of providing fast switching times, low on-state resistance, and high off-state resistance, all helpful in increasing efficiency [1].

In [1], Karabegovic examines class A, B, AB, C, D, and E amplifiers as to efficiency. The class E amplifier is identified as the most efficient for producing constant-frequency sinusoids. The reasons mentioned are that it is switch-mode and that it makes use of the parasitic capacitance of the switch as an integral part of the amplifier circuit. The highest practical power efficiency is found as 63% for a Class E amplifier operating at 10.6 GHz with a transistor as the switch. Karabegovic then performs simulations of a photoswitch-based amplifier with the results that anode efficiency is 80.1% and power-added efficiency is 59.3% at 10 GHz. Power-added efficiency is defined as:

$$\mathrm{PAE} = \frac{P_{RFout} - P_{RFin}}{P_{DC}} \quad , \qquad (1.1)$$

where P_{RFout} is the average power of the radio-frequency output, P_{RFin} is the power of the radio-frequency input signal, or, in this case, the power of the input optical signal, and

P_{DC} is the DC power applied to the amplifier. Anode efficiency, η, is the same as equation 1.1 without the P_{RFin} term.

1.1 SUMMARY OF CHAPTERS

This thesis contains seven chapters. Chapter 2 is concerned with background information relating to the other chapters and serves as a review of textbook-type information. It contains the following topics: types of photodetectors, properties of laser diodes, ray matrix analysis in optical systems, and microelectronic fabrication.

Chapter 3 covers the design process for the photoswitch to be used as the switching element in the class E amplifier. Linear vs. Avalanche action and gallium arsenide vs. silicon as a photoswitch material are topics initially covered. Choosing the general photoswitch geometry is described. A metal-semiconductor-metal photodiode general geometry is chosen. Then particular dimensions of the photoswitch are worked out. After that, breakdown voltage and minimum laser spot size are calculated for use in later chapters. Finally, fabrication of the photoswitch is covered.

Chapter 4 develops and describes the apparatus used to generate the light of square-wave intensity that will be applied to the photoswitch. Different methods of laser modulation are compared and a system is chosen. Then, the mounting of the laser to maximize intensity is discussed and the focusing of the laser beam in free space is covered.

Chapter 5 describes the engineering of the microstrip class E amplifier. Class E amplifier theory is briefly covered. Then, a design of the amplifier is developed, using

lumped elements (discrete inductors and capacitors). This design is then translated into a microstrip transmission line design with the feature of harmonic suppression added, to complete the design of the class E amplifier.

Chapter 6 details the experimental set-up and the results obtained and discusses these results.

Finally, Chapter 7 proposes new research directions for future work on this project.

CHAPTER 2

THEORETICAL BACKGROUND

The material in this chapter is meant as a review and sections can be skipped depending on familiarity to the reader.

2.1 PHOTODETECTORS [2], [3]

There are various ways of converting a light signal into an electrical signal for use by the class E amplifier. They include thermal detectors, photoelectric detectors, junction photodiodes, and photoconductors.

Thermal detectors rely on heating of an absorbing substance and converting the heat to electricity using a thermocouple or bolometer. A bolometer is composed of a substance that changes resistance with heat. Thermal detectors are either easily damaged (small absorbing region) or slow (large absorbing region).

Photoelectric detectors rely on the photoelectric effect. Photons are incident on an emitter plate, which then ejects electrons. These electrons are then accelerated by an electric field and picked up by a grid, thereby generating current. In a photomultiplier tube, there is also gain. The original electrons are accelerated to another plate, called a dynode, that ejects additional electrons after the collision. Multiple dynodes can be used for more gain. The drawbacks of photoelectric detectors are size and voltage required. A low-voltage photoelectric detector might require 300 volts to operate.

Junction photodiodes, particularly PIN photodiodes, are widely used for photodetection. To operate a PIN photodiode as a photoswitch (the application in this work), the diode is reverse biased for a low off-current. The depletion region extends across the relatively large I (intrinsic) region. A photon absorbed in the depletion region is converted to one electron and one hole for a net of one electronic charge of photocurrent. Often the I region is approximately one absorption depth in length, with the light entering along this length direction (they have one transparent contact). Since carriers must traverse, on average, half of this length, there is a limit on the speed of PIN photodiodes (see figure 2.1).

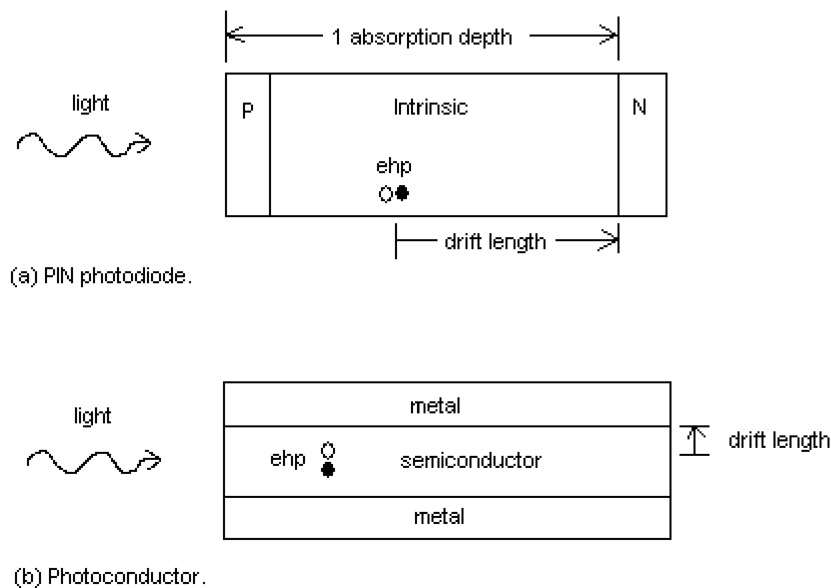

Figure 2.1. Comparison of drift length in (a) PIN photodiode and (b) photoconductor. Electon-hole pairs (ehp) generated have farther to drift in (a).

Finally, a photoconductor functions as a resistor with resistance dependent on light intensity. In its simple form, a photoconductor is a block of semiconductor with two

metal contacts. Assuming no recombination of electrons and holes, the photocurrent produced is

$$I_{ph} = q(\frac{\eta P_{in}}{h \upsilon}) \tag{2.1}$$

where q is the protonic charge, η is the quantum efficiency (number of electron-hole pairs produced per photon), P_{in} is the optical power, h is Planck's constant, and υ is the frequency of the light. Using spacing of electrodes, because of lower drift length and therefore drift time, an essentially arbitrarily high speed of response is possible, an advantage over PIN photodiodes (figure 2.1), and size, operating voltage, and damage threshold are not big issues, making the photoconductor superior to the rest of the photodetectors considered above. An example of a photoconductor is an MSM photodiode, detailed in chapter 3.

2.2 LASER DIODE [2], [3]

2.2.1 Laser Diode Basics

A semiconductor laser diode is used as the light source in this work. A diode laser is a two-energy-level system with the upper level being the conduction band and the lower level being the valence band of the semiconductor. The wavelength of emitted light then corresponds to the band gap energy of the semiconductor. Typical with diode lasers, the laser here is direct band gap, meaning the energy vs. momentum graph of the energy bands has a conduction band minimum at the same momentum as the valence

band maximum, allowing an energy jump of electrons without a change in momentum, thus a radiative transition.

While it is possible to externally pump (photopump) laser diodes to create population inversion (more than equilibrium number of electrons at the upper energy state), in this case internal (electrical) pumping of the PN-junction is used. The junction is forward biased resulting in a region where electrons and holes coexist with an energy difference approximately equal to the bandgap and their recombination produces light. The amount of light produced is then a direct function of the current through the diode.

2.2.2 Fabry-Perot Etalon

The diode laser used has a resonator that is rectangular in shape with polished ends. This is a form of a Fabry-Perot etalon, which is common in lasers. As mentioned, emission from the PN junction occurs near the bandgap energy. The spectrum emitted is still somewhat broad, as with an LED (light-emitting diode). To narrow the spectrum and greatly increase the coherence (quality of being in-phase) of the light, a Fabry-Perot etalon can be used. Light is then confined to narrow-band wavelength ranges where an integral multiple of half-wavelengths fit in the laser cavity. This is because for other wavelengths, a corresponding standing wave is not produced in the etalon and light interferes destructively or less constructively. The higher the reflection coefficient of the output facet of the etalon, the narrower the wavelength bands (linewidth) of the laser.

The etalon, along with the process of stimulated emission, allows for high coherence of the laser light as well. Stimulated emission is the generation of a photon

associated with a preexisting photon. The generated photon has almost exactly the same wavelength, direction, and, notably, phase as the previously existing photon. Cycling the same photons back and forth in the etalon therefore results in highly coherent light.

2.2.3 Beam Waist and Optical Confinement

An important variable in the focusing of laser beams is the beam waist w(z), which is the transverse distance from the center of the beam to its 1/e intensity points. It is given by

$$w^2(z) = w_0^2(1 + (\frac{\lambda_0 z}{\pi n w_0^2})^2) \quad (2.2)$$

where w_0 is the minimum beam waist, taken to occur at z = 0, z is the length along the beam, λ_0 is the free-space wavelength of the beam, and n is the refractive index of the medium (in this case, air). An important thing to notice about this equation is that the smaller w_0 is, the quicker the beam diverges. The upshot of this fact for the laser considered is that since the cavity or aperture of the laser is much wider than it is tall, the laser beam will be tall and small in width.

Since the cavities in diode lasers are so small transverse to the light direction (small size is an advantage in the eventual application here), confinement of the photons is desired. This amounts to employing heterostructures with an index of refraction profile of a waveguide to keep the photons from escaping from the side of the laser. Often, confinement of the carriers is accomplished by the heterostructures as well.

2.3 RAY MATRICES FOR OPTICAL SYSTEMS [2]

Because analysis of multiple lens systems can be complex, a ray matrix method was developed which keeps track of location and slope of rays. Ray matrices are also applicable to Gaussian beams as used in the Gaussian ABCD law, used in chapter 4. A ray matrix represents the effect that elements between a first transverse plane with a ray of radial location r_1 and slope r_1' and a second transverse plane, of resulting ray location r_2 and slope r_2', have on this ray:

$$\begin{bmatrix} r_2 \\ r_2' \end{bmatrix} = \begin{bmatrix} A & B \\ C & D \end{bmatrix} \begin{bmatrix} r_1 \\ r_1' \end{bmatrix}. \tag{2.3}$$

Combining two or more ray matrices for series elements is simply done by reversing their order (the matrix corresponding to the element first encountered by light is the matrix farthest to the right) and multiplying.

2.3.1 Ray Matrix for a Distance d

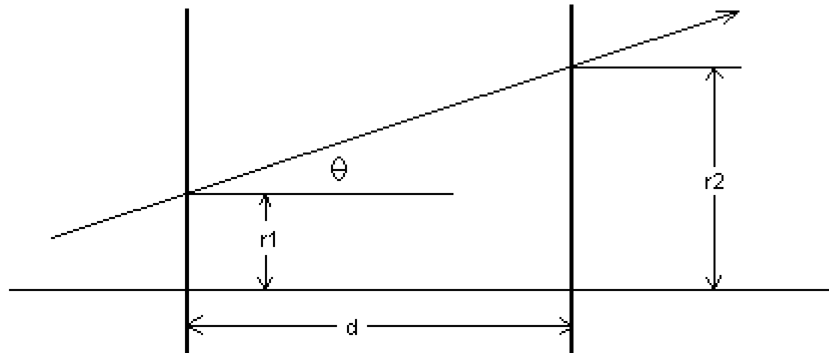

Figure 2.2. Diagram for calculating ray matrix for a distance d.

Consider calculating the ray matrix for a distance d of free space (fig. 2.2). The location $r_2 = r_1 + d \tan\theta$ but the slope $r_1' = \tan\theta$, so $r_2 = r_1 + d\, r_1'$. The slopes are the same, so $r_2' = r_1'$. In short, the ray matrix is

$$\begin{bmatrix} A & B \\ C & D \end{bmatrix} = \begin{bmatrix} 1 & d \\ 0 & 1 \end{bmatrix} \tag{2.4}$$

2.3.2 Ray Matrix for a Thin Lens

The ray matrix for a thin lens can be calculated by looking at two test rays: one that is collimated (parallel to the axis of the optical system) before the lens and passes through the focal point after the lens, and one which passes through the focal point before the lens and is collimated after the lens. The slope of the ray exiting the lens is given by

$$r_2' = Cr_1 + Dr_1'. \tag{2.5}$$

Considering a collimated ray entering the lens and passing through the focal point after the lens, the slope of the exiting ray is

$$r_2' = -\frac{r_1}{f}. \tag{2.6}$$

Since $r_1' = 0$, this gives $C = -1/f$. Considering a ray passing through the focal point before the lens and exiting it collimated,

$$r_1' = \frac{r_1}{f}. \tag{2.7}$$

Substituting these parameters into equation 2.5 gives

$$r_2' = -\frac{1}{f} r_1 + D\frac{r_1}{f}. \tag{2.8}$$

or $D = 1$. Since the position doesn't change ($r_2 = r_1$), the ray matrix for a thin lens is

$$\begin{bmatrix} A & B \\ C & D \end{bmatrix} = \begin{bmatrix} 1 & 0 \\ \frac{-1}{f} & 1 \end{bmatrix}. \tag{2.9}$$

2.4 MICROELECTRONIC FABRICATION [4]

The science of manufacturing electronic devices with features having dimensions on the micron or even sub-micron scale is called microelectronic fabrication. Only the topics in microelectronic fabrication applicable to the photoswitch in this study are covered.

2.4.1 Photolithography

Photolithography is the transferring of information on a photomask to a substrate wafer. A photomask is a transparent plate, often of fused silica, with a pattern on one side that is opaque, often made of chromium, that blocks light where the pattern is and lets it through where the pattern is not.

In photolithography, the substrate wafer is coated with photoresist on the top surface. The wafer is spun about an axis normal to the wafer surface and through its center at high speed (e.g., 2000 rpm) to allow the liquid photoresist to coat the surface of the wafer at uniform thickness. After this, the photoresist is soft-baked (e.g., 95º C) to harden it. Then the wafer is placed in an aligner, with the photomask above it, sometimes touching it, with the patterned (chromium) side next to the photoresist (contact lithography). The aligner then delivers a dose (J/cm^2) of ultraviolet light through the mask, onto the wafer. Next, the wafer is removed from the aligner and placed in a developer solution which removes photoresist in the pattern of the photomask. In a positive-tone photoresist, the exposed photoresist is removed; in a negative-tone

photoresist, the unexposed photoresist is removed. Exposure either breaks down polymers (positive-tone) or increases bonding (negative-tone). Finally, the photoresist is hard baked (higher temperature than soft-bake) to further increase its strength and stability.

2.4.2 Wet vs. Dry Etching of the Semiconductor Substrate

There are two technologies available for the etching of the semiconductor substrate: wet (chemical) etching, and dry (plasma) etching. Wet etching is accomplished using a liquid solution with chemical etchants, and the etching is isotropic (the same speed in all directions), so a wet etchant etches some distance underneath the photoresist. Dry etching is accomplished using a plasma, often chlorine- or fluorine-based and results in vertical sidewalls from the photoresist edge. Typical etch patterns are shown in figure 2.3.

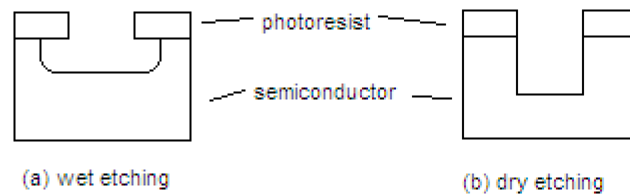

Figure 2.3. (a) Wet etching vs. (b) dry etching.

2.4.3 Metal Deposition

Ways to deposit metal on a semiconductor include electroplating, chemical vapor deposition, and physical deposition. Electroplating involves coating the substrate with a seed metal, depositing a patterned photoresist, growing metal on the exposed seed metal in a solution with the metal to be deposited at one electrical potential and the wafer at another, removal of the photoresist, and etching the seed metal that was under the photoresist. This technique is appropriate for depositing a thick layer of metal. Chemical vapor deposition (CVD) is also used when high aspect ratio (depth over width) features need to be covered. CVD involves chemical reactions of a gas or gases to produce the deposited product. The reactions are facilitated by heat, a plasma, or optical exposure.

Because of availability, physical deposition was used in this study. It comes in two varieties: evaporation and sputtering. The older method, evaporation, involves heating a charge (metal lump) in a chamber of high vacuum containing the wafer. The metal vaporizes and is deposited throughout the chamber. The newer method, sputtering, has better step coverage than evaporation (though not as good as electroplating or CVD). In sputtering, high-energy ions strike a negatively charged target to be deposited. The target atoms are ejected with high energy and move through the moderate vacuum to the substrate wafer. Substrate heat or bias further improves step coverage.

2.4.4 Liftoff vs. Etching for Metal Patterning

There are two possible fabrication processes to produce a metal pattern on top of the semiconductor wafer in conjunction with physical deposition: liftoff and etching. Liftoff (figure 2.4) is performed after a patterned photoresist is deposited and then a metal layer is deposited on top of that. The wafer is put into acetone, which dissolves the photoresist and removes the metal above it, if the liftoff works correctly. Alternatively, etching can be used (figure 2.5). The metal is deposited first, then the patterned photoresist. An etchant is then used that etches the metal, but not the photoresist or semiconductor. The wafer is submerged in the etchant until the exposed metal is gone. Acetone is then used to remove the photoresist. The result of either process is a metal pattern on the top surface of the semiconductor.

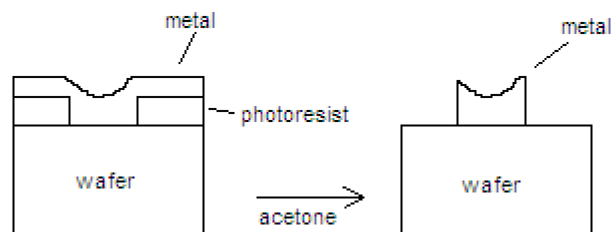

Figure 2.4. Liftoff.

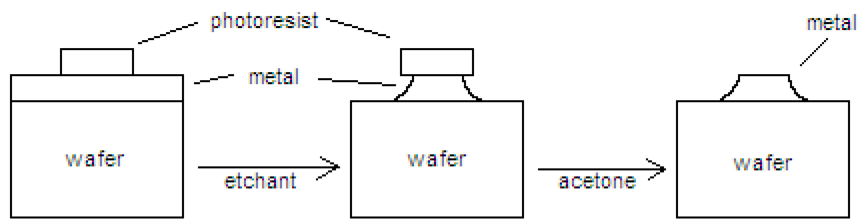

Figure 2.5. Metal etching.

CHAPTER 3

PHOTOSWITCH DESIGN

A photoconductive semiconductor switch, referred to as "the photoswitch" from now on, is simply a device that conducts at low resistance from one of its terminals (the anode) to the other terminal (the cathode), with an anode-to-cathode bias, when sufficient light is applied to it and serves as an essentially open circuit with respect to the terminals when the light source is off. Linear photoswitches contribute at most one electron and one hole to current for each photon absorbed and avalanche photoswitches provide some gain to the photocurrent, so that many electron-hole pairs are derived from each photon.

In this design linear was chosen over avalanche photoswitch action because of higher speed and lower jitter (uncertainty of a switching event in time) of linear over avalanche photoswitches. In keeping with [1], a simple electrode / intrinsic semiconductor / electrode scheme was opted for and the semiconductor material chosen was gallium arsenide (GaAs). Compared to silicon, GaAs's high breakdown fields, high drift velocity, high mobility, high maximum current density, and very large "off" or dark resistivity recommend its use as a photoswitch material. High breakdown field translates to a higher possible off-state voltage and, thus, output power. High drift velocity results in fast switching. Since mobility is the slope of the carrier velocity - electric field curve at low electric field and since, during the on state, the voltage and therefore the electric field across the switch is very low, higher mobility results in lower on-state resistance for

a given optical energy [5]. Higher maximum current density translates to a higher possible on-current. Finally, large dark resistivity results in a lower off-current.

3.1 BULK VS. LT GaAs

Bulk (standard) GaAs is now compared to low-temperature-grown (LT) GaAs for use as a photoswitch material. It is hypothesized that sweep-out of carriers is the limiting factor in the switch-off time for bulk GaAs, and that recombination time is the limiting factor in LT GaAs. Calculation of carrier dynamics is generally a problem for computer simulation, but given a couple of simplifying assumptions, a closed-form equation can be used to approximate carrier dynamics. For bulk GaAs, then, the equation for holes is considered, since holes move more slowly than electrons in GaAs. If the hole sweep-out time is shorter than the recombination-related time, then so too will be the electron sweep-out time. The simplifying assumptions making a closed-form equation possible are that carriers are generated at time t = 0 and in the plane x = 0. The resulting equation is [6]:

$$p(x,t) = \frac{A}{(4\pi D_p t)^{1/2}} e^{-t/\tau_R} \exp\left(\frac{-(x - v_{dp} t)^2}{4 D_p t}\right) \qquad (3.1)$$

where p(x,t) is the hole concentration and is assumed to be far above the equilibrium value (which is low for intrinsic GaAs), A is a constant representing the number of holes injected, D_p is the hole diffusion coefficient, t is time, τ_R is the recombination time, x is the distance from the injection point, and v_{dp} is the hole drift velocity. A saturation drift velocity of $7\text{x}10^6$ cm/sec [7] will be assumed, corresponding to the high voltage across the switch at the beginning of the off-state. For bulk GaAs, D_p =10.4 cm^2/sec and τ_R =

10^{-7} sec [7]. The equation has three terms: a constant, an exponential with τ_R that monotonically decreases from 1 with t, and an exponential with v_{dp} that increases to 1 at $x = v_{dp}t$ and then decreases with t from then on. The constant is just a scaling factor and solutions can be normalized to remove this factor, so the real question is, when does one or the other of the exponentials decrease to e^{-3} (5% of the maximum value), representing turn-off? x = 0.5 μm will be considered, to represent the sweep-out length of the switch designed in Karabegovic's simulations [1]. Given all the inputs, the first exponential reaches e^{-3} at t = 300 ns and the second exponential reaches e^{-3} (after peaking) at t = 12.9 ps. This shows that, indeed, carrier sweep-out is the shorter, limiting time for turn-off in bulk GaAs, as hypothesized, and that, if turn off relied on recombination, it would take 23,000 times as long.

Next, we consider LT GaAs. This time, electrons (not holes) are considered, to make sure the recombination time is the dominating factor, even over the faster type of carrier. The equation is [6]:

$$n(x,t) = \frac{A}{(4\pi D_n t)^{1/2}} e^{-t/\tau_R} \exp\left(\frac{-(x - v_{dn}t)^2}{4 D_n t}\right) \qquad (3.2)$$

where the parameters for holes are replace by those for electrons. Parameters for LT GaAs are [8]: $D_n = 77.6$ cm^2/sec, $\tau_R = 200$ fs, and $v_{dn} = 10^7$ cm/sec. The first exponential reaches e^{-3} at t = 600 fs and the second exponential reaches e^{-3} (after peaking) at t = 1.79 ps. Indeed, as hypothesized, the LT GaAs device is limited by the recombination time, and sweep-out takes approximately 3 times as long.

Since the LT GaAs device is recombination-time limited, many carriers will recombine before reaching the electrodes, resulting in more light power required and thus

a lower PAE. For this reason, bulk GaAs was chosen over LT GaAs, ensuring that the vast majority of photocarriers will be converted to switch current.

3.2 GENERAL PHOTOSWITCH GEOMETRY

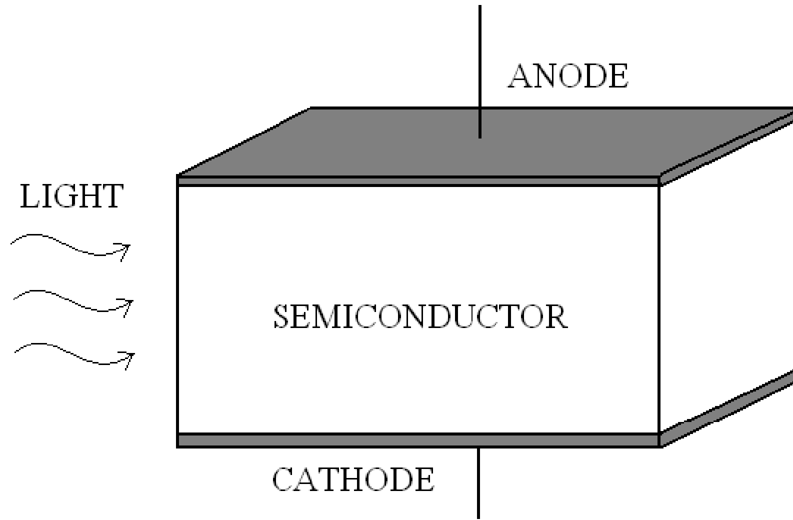

Figure 3.1. Photoswitch design in [1].

Karabegovic's design [1], figure 3.1, incorporated parallel plates with GaAs in between at a thickness on the order of 1 μm. To keep laser-photoswitch alignment and coupling a simple issue, the geometry chosen for the photoswitch in this paper was what is known as a metal-semiconductor-metal (MSM) photodiode, a widely adopted but unfortunate name, since this type of device does not act as a conventional diode and is only one specific instance of the metal-semiconductor-metal scheme. A MSM photodiode is shown in figure 3.2 [9]. These devices have fast response and simple structure compared to other photodetectors of the same active area such as P-i-N structures [10], [11]. The MSM photodiode is fast because of the interdigitated structure,

which reduces carrier transit time by the close spacing of electrodes, while maintaining a large active area. This large active area is what makes the alignment of the laser-photoswitch pair manageable, with simple focusing of the laser beam and manual adjustment of the location of the photoswitch sufficient for maximal coupling of the laser power.

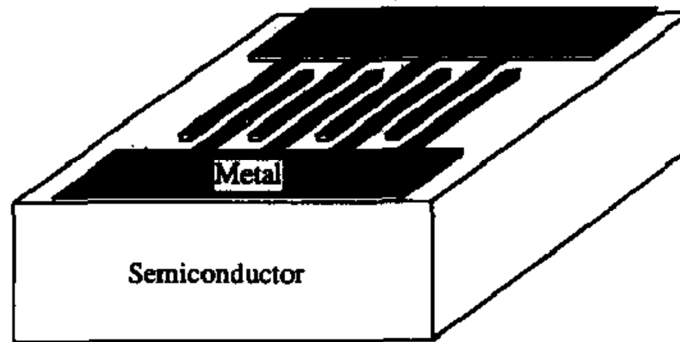

Figure 3.2. MSM photodiode

An original intention in the design of the photoswitch was to have the electrodes penetrate downward into the GaAs so that the fingers in figure 3.2 would be more like vertical parallel plates, inside the semiconductor. The purpose of this design feature is to speed up the device, since, if the depth of the electrodes is a few absorption depths or more, most of the photocarriers would proceed along short, almost straight paths to the electrodes. With surface electrodes as in figure 3.2, on the other hand, the electric field that passes through the more deeply generated electron-hole pairs traces arc-like lines to the distant electrodes. (An advantage of more shallow electrodes, however, is that capacitance per unit length, C', between any two electrodes is smaller, since C' is proportional to depth of electrodes divided by electrode separation.) Unfortunately,

because of a local lack of dry etching for GaAs, it was not possible to have deep electrodes which would make contact with the GaAs on the sides of the electrodes. It was, however, possible, using wet etching, to etch a small distance into the GaAs and have electrical contact at the bottom of the electrodes, to achieve a geometry as in figure 3.3, taken from [12]. While [12] uses low-temperature-grown GaAs, which increases speed but decreases photocurrent compared to bulk GaAs, the geometry of the device in [12] is very similar to that of the device developed here. Compared to a similar device with electrodes on the surface, the recessed electrode structure had a 25% breakdown voltage and sensitivity increase, improved speed, and much improved capacitance. The optimized depth was found to be 180 nm. For the device here, because bulk GaAs is used, which has a longer carrier lifetime than low-temperature-grown GaAs, meaning more charge might accumulate in the upper region of the semiconductor, a reduced electrode depth of 100 nm was decided upon.

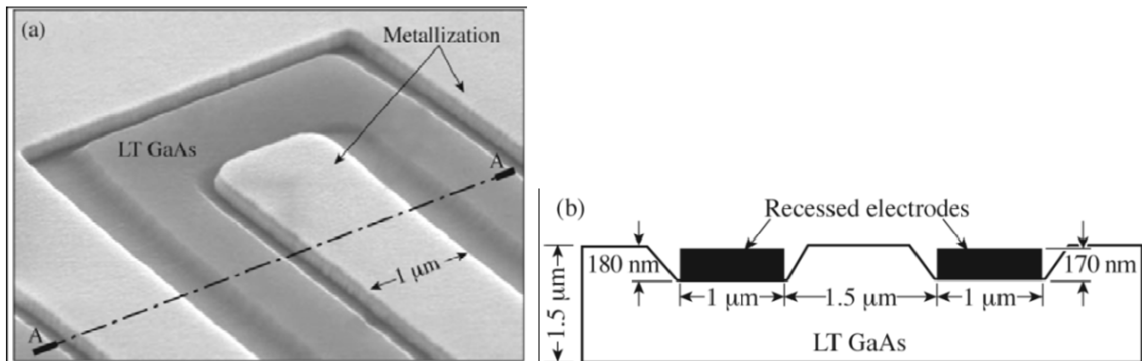

Figure 3.3. New recessessed electrode geometry from [12]. (b) is section A-A from (a).

In summary, Karabegovic's photoswitch design [1] is compared to the adopted MSM photodiode, in table 3.1.

	Karabegovic [1]	MSM photodiode chosen
Figure	figure 3.1	figure 3.3
Active area	small	large
Ease of alignment	difficult to align	easy to align
Penetration of electrodes	deep	shallow
Paths of deeply generated carriers	short, straight	long, curved
Capacitance per unit length along an electrode	high	low

Table 3.1. Comparison of photoswitch in [1] with the adopted MSM photodiode.

3.3 FINGER WIDTH AND SPACING AND ACTIVE AREA

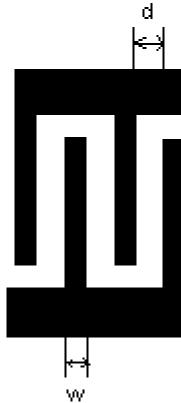

Figure 3.4. Finger width, w, and spacing, d. Black represents electrodes.

The next step in the design of the photoswitch was to determine the electrode width, w, and spacing, d (figure 3.4). In [1] it was demonstrated that for a parallel-plate device, a spacing of 0.5 μm was appropriate for 10 GHz operation. The electrode width should be kept as small as possible to reduce waste of the light incident on the device. Because of fabrication constraints, the minimum electrode width and spacing were both 1.5 μm, so this value was adopted for both. This means that the device will operate at

around 3 GHz or less, assuming carrier transit time scales with 1/distance, though the speed is probably somewhat less, because of the lack of depth of the electrodes.

The final major step in the design of the device is to determine the active area. The larger this is, the easier it is to align the photoswitch with the laser, but also the larger the capacitance. In [12] it was found that the capacitance of the recessed electrode geometry was a mere 28% of the capacitance of a similar surface electrode structure. From a conformal mapping procedure using elliptic integrals [9], the capacitance per unit length, C', between two fingers of the surface electrode geometry was found to be 0.06 fF/μm, which translates to 0.017 fF/μm for the recessed geometry. The total capacitance of the photoswitch is given by [9]:

$$C = C'A/(d + w) \tag{3.3}$$

where A is the area of the active region, containing all the fingers, and $d + w = 3$ μm is the spacing plus the width of the electrodes. For the class E amplifier at 3 GHz, the total capacitance of the switch, C, according to [1], should be less than or equal to 190 fF. This gives an upper bound on A of 33,500 μm^2 or a square of side length $L = 180$ μm. The area can be smaller than this and probably should be to eliminate any problems resulting from approximation or use of an altered class E amplifier. The requirement that the photoswitch have a large enough active area to be aligned relates to the graduation on the micropositioner obtained for this project, which is 2.5 μm. Choosing an active area of side length at least ten times this should be sufficient, giving a side length of $L = 25$ μm. So, $25\ \mu m \leq L \leq 180\ \mu m$ and $L = 75$ μm was chosen. This allows space for 12 fingers on each electrode of lengths ≈ 75 μm. This translates to a capacitance of $C =$ 31.9 fF (112.5 fF for the similar surface electrode geometry).

3.4 BREAKDOWN VOLTAGE

After the basic design of the photoswitch, certain parameters and checks have to be investigated to correctly implement the photoswitch in a circuit. First of all, breakdown voltage, V_{BD}, should be ascertained. Breakdown can occur on the surface (flashover) or in the bulk of the semiconductor, and each phenomenon has its own breakdown field, E_{BD}. For GaAs, the bulk breakdown field is approximately 300 kV/cm [14] and the surface breakdown field is approximately 140 kV/cm [5]. The recessed-electrode design creates a longer, more difficult path for surface breakdown to occur across, so the breakdown field of the device should be somewhere between the surface and bulk values. Using the electrode spacing, d = 1.5 μm to calculate

$$V_{BD} = d\, E_{BD} \tag{3.4}$$

gives $21\text{ V} \leq V_{BD} \leq 45\text{ V}$. The result is probably closer to the lower voltage as in [12]. The breakdown voltage represents the maximum off-state voltage that can appear across the switch.

3.5 LASER SPOT SIZE

The current density must remain below the maximum current density, at which thermal runaway occurs and the device is damaged. The value of the maximum current density is given by [5]:

$$J_{max} = n_c\, q\, (v_{dn} + v_{dp}) \tag{3.6}$$

where q is the protonic charge; v_{dn} and v_{dp} are the drift velocities of electrons and holes, respectively; and n_c is the maximum carrier density allowed for electrons or holes and is determined experimentally. Assuming n_c to be about the same for GaAs as it is for silicon, for which the value is approximately known, then $n_c = 5x10^{17}$ cm^{-3}, as limited by thermal runaway, auger absorption, and free carrier absorption. Substituiting a conservative value of $6x10^6$ cm/sec for $v_{dn} + v_{dp}$ in GaAs gives $Jmax = 500$ kA/cm^2 [5]. The photoswitch considered here is illuminated on the top surface, at which the intensity of light is higher than it is deeper down because of absorption, so the photogenerated current will have a maximum near the top surface of the device. It is necessary to determine the maximum incident light intensity, I_{0max}, given the maximum allowable current density, $J_{max} = 500kA/cm^2$.

The intensity of light a distance x into an absorbing medium is $I = I_0e^{-\alpha x}$, where I_0 is the intensity just inside the illuminated surface and α is the absorption coefficient of the medium. The total intensity absorbed before reaching x is

$$I_{abs} = I_0 - I = I_0(1- e^{-\alpha x}). \quad (3.7)$$

The intensity absorbed per unit x is then,

$$\frac{dI_{abs}}{dx} = I_0\alpha e^{-\alpha x}. \quad (3.8)$$

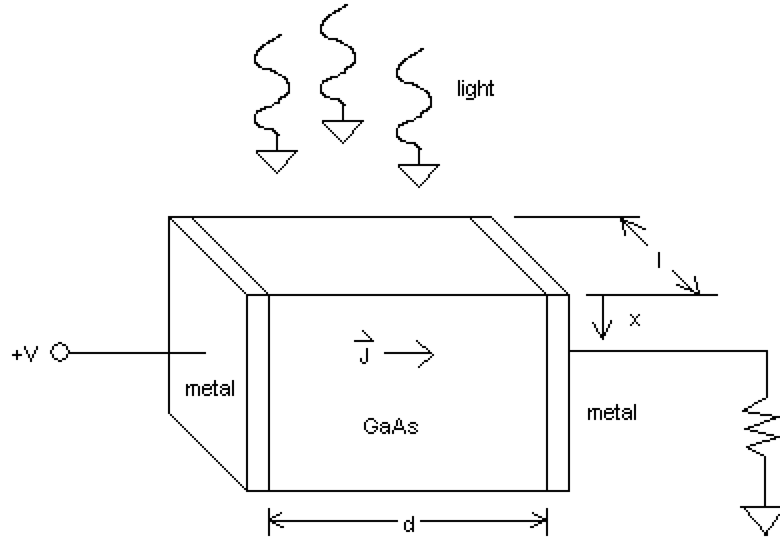

Figure 3.5. Variables used to calculate maximum light intensity.

At x = 0, then,

$$\frac{dI_{abs}}{dx} = I_0\alpha \approx \frac{\Delta I_{abs}}{\Delta x} \tag{3.9}$$

where ΔI_{abs} is the intensity of light absorbed over a small distance Δx into the medium.

In equation 3.9, $\Delta I_{abs} = E/(tA)$, where E is the energy of the n photons absorbed in Δx, i.e., $E = nh\nu$, with $\nu = c/\lambda$; h is Planck's constant, ν is the frequency of the light, c is the speed of light in vacuum, λ is the vacuum wavelength of the light, t is the time of exposure, and A is the area of exposure, i.e., A = ld, the length times the width of the exposed area (see figure 3.5). Therefore,

$$\Delta I_{abs} = \frac{nhc}{tld\lambda} = \alpha I_0\, \Delta x \ . \tag{3.10}$$

Assuming, to be conservative, 100% internal quantum efficiency, n photons absorbed in Δx produce n carriers of absolute charge q each (protonic charge). The current density J (see figure 3.5) is then

$$J = \frac{nq}{tl\,\Delta x}\ . \qquad (3.11)$$

Using equations 3.10 and 3.11, $I_0 = \frac{hc}{q\alpha d\lambda} J$, so $I_{0max} = \frac{hc}{q\alpha d\lambda} J_{max}$. (3.12)

For GaAs, J_{max} = 500 kA/cm^2 and for λ = 830 nm (see chapter 4), α = 1.2 μm^{-1}, so given d = 1.5 μm, I_{0max} = 415 kW/cm^2 .

As will be shown in a later chapter, the total power of the light beam entering the semiconductor will not exceed 400 mW, so assuming a uniform intensity cross-section of the beam, the smallest allowable spot size is 96 μm^2. Assuming an approximately Gaussian beam, which has an intensity at the center of not more than three times the average intensity of the spot, a safe spot size would be 286 μm^2 or a diameter of 20 μm. These values represent the smallest the laser spot on the active area of the photoswitch should be, to avoid current filamentation.

3.6 PHOTOSWITCH ANALYSIS AND PERFORMANCE SUMMARY

A number of parameters for the photoswitch remain to be determined, including turn-off time, turn-on time, off-state resistance, and on-state resistance. First of all, the turn-off time, $t_{off} = t_{drift}$, needs to be determined. Using the methods of Section 3.1, the equation to determine t_{drift} is given by:

$$\frac{-(x - v_{dp}\, t_{drift})^2}{4\, D_p\, t_{drift}} = -3 \tag{3.13}$$

This time x = 2d = 3 μm, because of the longer drift length in the recessed-electrode MSM photodiode. $v_{dp} = 7\text{x}10^6$ cm/sec and $D_p = 10.4$ cm^2/sec, as before. The result is:

$$t_{off} = t_{drift} = 54.7 \text{ ps}. \tag{3.14}$$

Next, we will consider the off-state resistance, which is given by [1]:

$$R_{off} = \frac{(2d)}{(n_0\, \mu_n + p_0\, \mu_p) q\, (0.5\, w) L} \tag{3.15}$$

where 2d is used for the same reason as above, $n_0 = 5\text{x}10^{13}$ cm^{-3} for an unintentionally n-doped semiconductor assumed, p_0 is neglected compared to n_0, q is the protonic charge, (0.5 w) is assumed as the depth distance for the resistor area, and L = 0.1875 cm is the total length of the gap between the electrodes as the width distance of the resistor area. This gives:

$$R_{off} = 313\ \Omega \tag{3.16}$$

Now, we consider the on-state resistance, given by [1]:

$$R_{on} = \frac{(2d) E_\lambda}{L\, q\, (\mu_n + \mu_p)\, I_0\, t_{drift}} \tag{3.17}$$

where the variables are the same as above, except $E_\lambda = 2.39\text{x}10^{-19}$ J is the energy of an 830 nm photon, hole mobility $\mu_p = 400$ cm^2/(V sec) [7], and $I_0 = 7111$ W/cm^2 is the intensity of light applied to the switch for 400 mW of light power distributed evenly over the whole active area. The resulting on-state resistance is:

$$R_{on} = 0.689\ \Omega \tag{3.18}$$

Finally, the 0 to 90% amplitude turn-on time can be calculated [1]:

$$t_{on} = \frac{0.9\,(2d)\,E_{\lambda}}{R_{on}\, I_0\, L\, q\, (\mu_n + \mu_p)} = 49.3 \text{ ps.} \tag{3.19}$$

The following table summarizes the expected performance of the photoswitch:

parameter	symbol	value
electrode width	w	1.5 µm
electrode separation	d	1.5 µm
active area	A	5625 μm^2
breakdown voltage	V_{BD}	≥ 21 V
capacitance	C	≤ 112.5 fF
turn-on time*	ton	49.3 ps
turn-off time	toff	54.7 ps
on-state resistance*	Ron	0.689 Ω
off-state resistance	Roff	313 Ω

* @ 400 mW optical excitation distributed uniformly over the active area.

Table 3.2. Summary of parameters for the designed photoswitch.

3.7 PHOTOSWITCH FABRICATION

Images of the photomask for the photoswitch are given in Appendix B. Both the liftoff and etching techniques of metal patterning, mentioned in Chapter 2, using a positive-tone photoresist and a negative-tone photoresist, respectively, were attempted using the photoresist AZ5214 from AZ Electronics. With different processes of baking, the photoresist acts as either positive-tone or negative-tone. It was discovered that the negative-tone form of the photoresist was inferior and it didn’t yield remotely usable

photoswitches. The positive-tone form performed better, but it was determined that liftoff of metal for feature sizes of 1.5 μm was not possible. Preparations were made to move to a different lab and use a better negative-tone photoresist, but mechanical failures of metal deposition machines (evaporation and sputtering) in all labs prevented any further work.

A PIN photodiode was purchased to be used in place of the MSM photodiode as the photoswitch in this work because of the above fabrication problems. Its characteristics are inferior to what the MSM photodiode's were projected to be. The breakdown voltage of the PIN photodiode is 25 V, its maximum current is 10 mA, and, most notably, its capacitance is 4 pF.

CHAPTER 4

LASER CIRCUIT SETUP

4.1 WAVELENGTH

There are a few different ways to approach supplying the optical excitation to the photoswitch. This chapter covers the decisions made choosing the components up to and including the laser and focusing elements, but excluding everything that comes after these elements, such as the photoswitch and tank circuit of the class E amplifier. The first thing to be determined is the wavelength of the optical source. Given that the bandgap energy of GaAs is 1.43 eV, the largest wavelength that effectively produces electron-hole pairs is 867 nm. The absorption coefficient slowly increases as the wavelength decreases beyond this point, but the energy required to create a photon increases as well, so, in the interest of power-added efficiency, the wavelength should be kept below 867 nm, but not far below. In the interests of size, it was decided that a diode laser would be best.

4.2 LASER MODULATION

Next, the requirement for up to 3 GHz square-wave modulation of the optical signal must be met. Since pulsed lasers operate with duty cycles of much less than 0.5 and repetition rates well below the GHz range, some sort of external modulation of a

continuous-wave (cw) laser is necessary. There are two possibilities for external modulation: (1) optical modulation of the beam emitted by the laser, and (2) electrical modulation of the signal powering the laser.

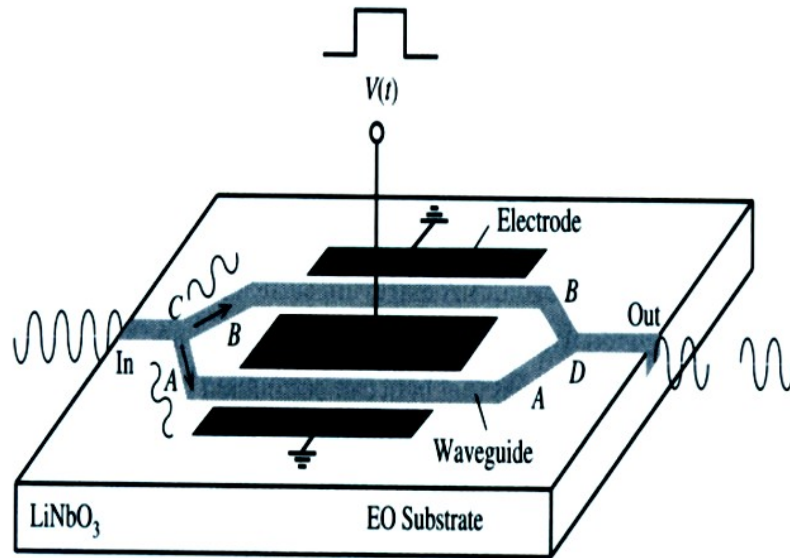

Figure 4.1. Mach-Zehnder intensity modulator.

Modulation of the beam emitted by the laser is accomplished with an electrooptic (EO) intensity modulator. EO intensity modulators usually come in the form of a Mach-Zehnder modulator (see figure 4.1 [15]), operating using the Pockels effect, whereby a change in electric field produces changes in the components of the refractive index of a crystal, proportional to the change in electric field. The modulator in figure 4.1 has light entering the EO material waveguide at the left, which is split into two beams, A and B, at C. Then the separated waveguides experience opposite electric field because of the arrangement of the applied voltage and the two ground terminals. This causes opposite changes in the applicable refractive indices for the two paths such that the speed of the optical signal, inversely proportional to refractive index, is higher for one path and lower

for the other, giving a phase difference ϕ between the signals. The paths are brought back together at D and interfere constructively or destructively. The formula for output optical power is:

$$P_{out}(\phi) = \cos^2\phi \; P_{out}(0) \tag{4.1}$$

Where $P_{out}(0)$ is the output for zero phase difference, i.e. V = 0. The input to the modulator must be polarized for the modulator to work.

Commercially available EO intensity modulators for around 800 nm light have a maximum input light intensity of 5 mW. At 1550 nm, however, the maximum input intensity is 500 mW to 1 W. For 100% quantum efficiency, photoswitch current is

$$I = \frac{q\,\lambda\,P}{h\,c} \tag{4.2}$$

Where q is the magnitude of electronic charge, λ is wavelength, P is the optical power, h is Planck's constant, and c is the vacuum speed of light. For an 800 nm EO intensity modulator, then, the maximum photoswitch current is 3.2 mA. Assuming a 50 Ω load, this translates to 0.16 V as a maximum load voltage, which is far too low. This leaves two possible options if optical modulation is going to be pursued: (1) the modulated signal at 800 nm can be amplified optically, or (2) 1550 nm light can be used and then frequency doubled to 775 nm. As it turns out, commercially available optical amplifiers at around 800 nm have a maximum output of around 3 mW, less than the power of the signal we are trying to amplify, so modulating the output of an approximately 800 nm laser is not an option.

The two options left are (1) using an optical modulator at 1550 nm and doubling the frequency of the signal, and (2) modulating the electrical power source of the laser. Schematic diagrams of two possible excitation systems are shown in figure 4.2.

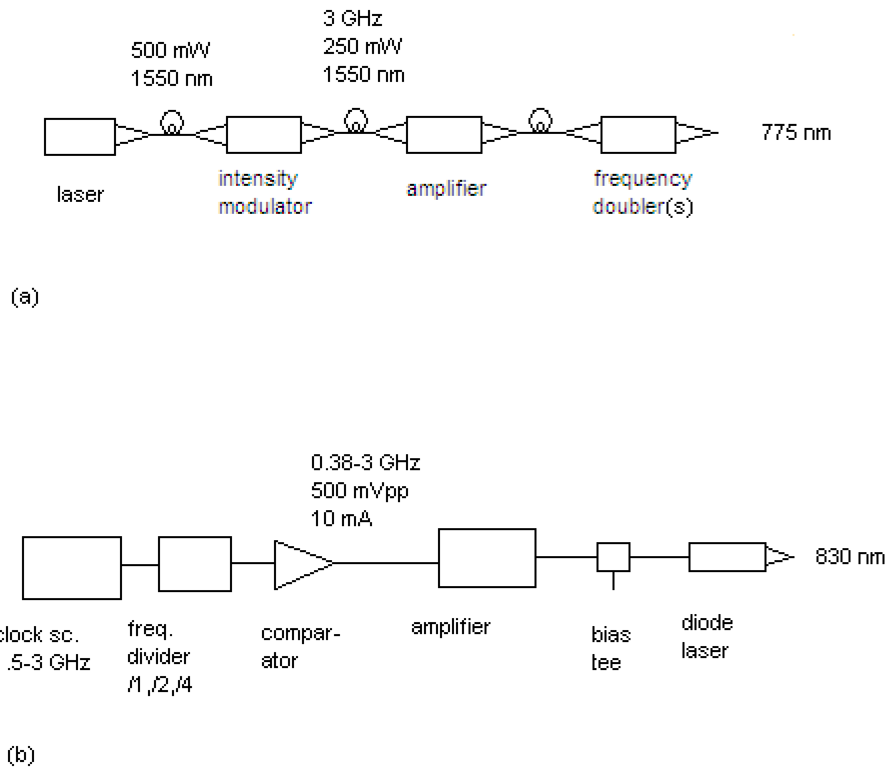

Figure 4.2. (a) 1550 nm laser system. (b) 830 nm laser system.

4.2.1 Frequency-Doubled System

First, we will discuss the frequency doubled system, figure 4.2(a). We will assume an output optical peak power of 400 mW (a square wave alternating between 400 mW and 0 mW). A frequency doubling crystal is, at most, 10% efficient when converting 1550 nm power to 775 nm. The crystals themselves (periodically-poled lithium niobate) cost around $5000 each. Amplifiers range in price depending on the maximum output light power. The lowest-cost amplifier-doubler pair that produces 400

mW is a 2 W amplifier with two crystals, which costs a total of $21,000. Add to this the cost of the rest of the system and the cost would be $25,000 or more for the 1550 nm laser system. Note that even if ten frequency-doubling crystals are used, only 65% of the laser power is frequency doubled, and size and alignment of the ten crystals is an issue. Also, the crystals have to be kept at a controlled temperature. The frequency-doubling system is, however, capable of producing up to 6 W with two crystals (at a cost of $75,000) or, for example, 1W peak optical power with two crystals at a cost of $34,000.

4.2.2 Electrically Modulated System

Second, we move on to the electrically modulated system, shown in figure 4.2(b). The clock source - frequency divider pair produce an electrical signal of approximately 400 mV peak-to-peak at a range of 0.38 to 3 GHz frequency with fairly good rise/fall times. The comparator is included to clean up the signal, slightly increase the voltage to 500 mV peak-to-peak, and sharpen up the rise/fall times to a minimum of 50 ps. The 5 mW electrical peak power is then amplified by the high-frequency amplifier. Amplifiers of this type run about $1000 per watt of output. A bias tee is then used to bias the signal between laser threshold current and the upper current available, to maximize laser peak power (see section 4.4). The approximate cost of this system is $6000 or more for the 830 nm laser system.

4.2.3 Choice of Laser Circuit

The second system, the electrically modulated system, is easier to implement, more efficient, and less costly. The frequency doubling crystals are what make the first system more difficult to implement. They require temperature control and careful alignment. The first system also loses significant efficiency, especially if many frequency doubling crystals are not used. The cost of creating the square wave signal input into the EO intensity modulator wasn't even considered and the cost of a 400 mW system was already $25,000. If, on the other hand, the second system is chosen, the cost is only $6000. Therefore, the electrically modulated system, figure 4.2(b), was chosen.

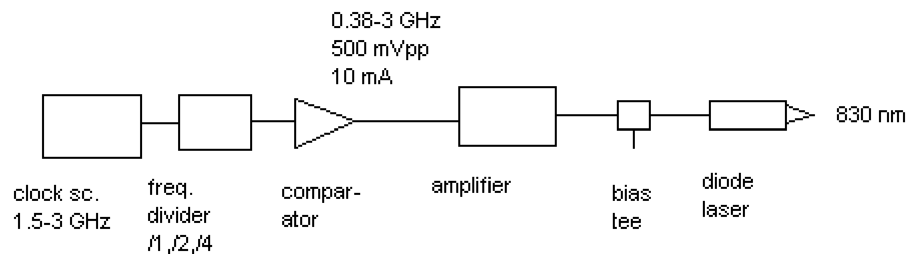

Figure 4.3. Chosen system: electrically modulated 830 nm laser system.

Figure 4.3 shows the chosen, electrically modulated, system again. It was found in implementing the system, as discussed below, that 400 mW peak laser power was not obtainable because of matching requirements with a laser load of 1 Ω, but, as discussed, the price is right. If the budget had permitted, a higher-power amplifier could have been used to make up the difference, still below the cost of the frequency-doubled system.

4.3 LASER MOUNTING

The difficulty in mounting the laser arises from its low impedance of 1 Ω. The electrical signal driving the laser arrives on a 50 Ω coaxial cable. This characteristic impedance can be shifted down to 10 Ω via a microstrip transmission line, but that is the minimum characteristic impedance recommended for microstrip implementation, even for low-to moderate frequency [16]. Given the Teflon composite circuit board obtained for this project of dielectric constant $\varepsilon_r = 2.5$ and thickness h = 1.5748 mm, the microstrip width w = 4.476 mm for 50 Ω characteristic impedance and w = 21.24 mm for 20 Ω. See Appendix A for the calculation of these strip widths. A smooth taper with slow change in conductor border slope between the two widths serves as an impedance translator of wide bandwidth [16].

The geometry adopted for the taper is what is known as a triangular taper (though it is not triangular in shape). For a triangular taper, the characteristic impedance of the strip, Z, is given by:

$$Z = Z_0 \exp\left(2(x/L)^2 \ln(Z_L/Z_0)\right) \quad \text{for} \quad 0 \le x \le L/2 \tag{4.3}$$

$$\text{and} \quad Z = Z_0 \exp\left((4x/L - 2x^2/L^2 - 1) \ln(Z_L/Z_0)\right) \quad \text{for} \quad L/2 \le x \le L$$

where Z_0 is the initial characteristic impedance, Z_L is the final characteristic impedance, L is the total length of the taper, and x is the distance along the taper. In [17], it is shown that reflection coefficients for a triangular taper are approximately zero for L/λ equal to an integer, where $\lambda = c/(\upsilon(\varepsilon_{eff})^{0.5})$ is the wavelength of the electrical signal in the line, and c is the vacuum speed of light, υ is the frequency, and ε_{eff} is the effective dielectric constant of the line, calculated by the method given in appendix A. The average of ε_{eff}

for 50 Ω and 20 Ω characteristic impedance is 2.215 so, using this average with $\upsilon = 2$ GHz yields $\lambda = 100.717$ mm. Setting L = 100.717 mm should work well, since the harmonics of the 2 GHz square wave will have wavelengths at approximately half, one third, one fourth, etc. of L, so the reflection coefficients will be essentially zero. The triangular taper used is shown in figure 4.4 (approximately actual size).

Figure 4.4. Triangular taper for laser mounting. Laser is mounted on the right side.

4.4 BIAS TEE REQUIREMENTS AND LASER DRIVE SIMULATION

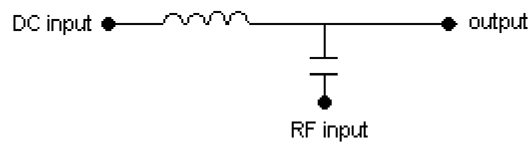

Figure 4.5. Bias tee.

As mentioned above, a bias tee is needed to translate the squarewave output of the RF amplifier up, to drive the laser, since the output of the amplifier has an average of zero volts. A bias tee, figure 4.5, simply adds the voltage of an RF input to a DC input to get the output. The inductor provides a constant current from the DC input, translating the DC input voltage to the average voltage of the output. The capacitor allows the RF input to be superimposed on this DC voltage. The goal of the bias tee here is to translate the off-state voltage of the amplifier from a negative value to a positive value just under laser threshold.

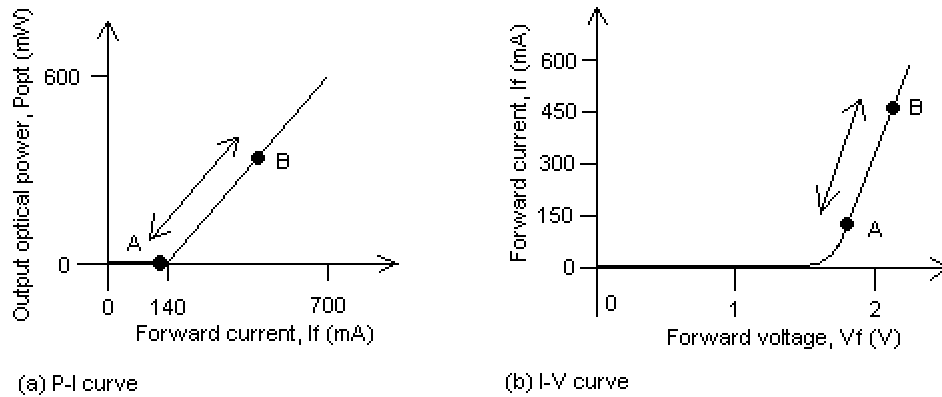

Figure 4.6. Bias ranges A-B for diode laser, given threshold current of 140 mA on P_{opt} vs. I_f graph (a). (b) is diode I_f vs. V_f curve.

Figure 4.6(a) shows the threshold current for the laser is at 140 mA, below which there is no optical output. The lower current of the square wave coming out of the bias tee, then, should be just under this, say 120 mA. The upper current can be at most 700 mA to avoid damaging the laser. Since the laser is mounted in series with enough resistance so the total load is approximately 30 Ω, the lower bias tee output voltage should be 3.6 V, and the upper voltage, up to 21 V. Since the RF amplifier has a maximum swing of approximately 10 $V_{p\text{-}p}$, the upper voltage will be 13.6 V, for an upper current of 453 mA. The DC input to the bias tee is then -5 V + 3.6 V = 8.6 V. The minimum values for bias tee parameters are given, then, in table 4.1.

input RF voltage	+/- 5 V
input DC voltage	8.6 V
input RF current	+/- 167 mA
input DC current	287 mA
input RF power	835 mW
input DC power	2.47 W
operational frequency range	0.1 to 10 GHz

Table 4.1. Minimum specifications for bias tee.

In figure 4.6, the segments A-B represent the operating range of the laser diode, the swing of the bias point.

Next, the laser drive circuit will be simulated using PSpice, including the bias tee and its load.

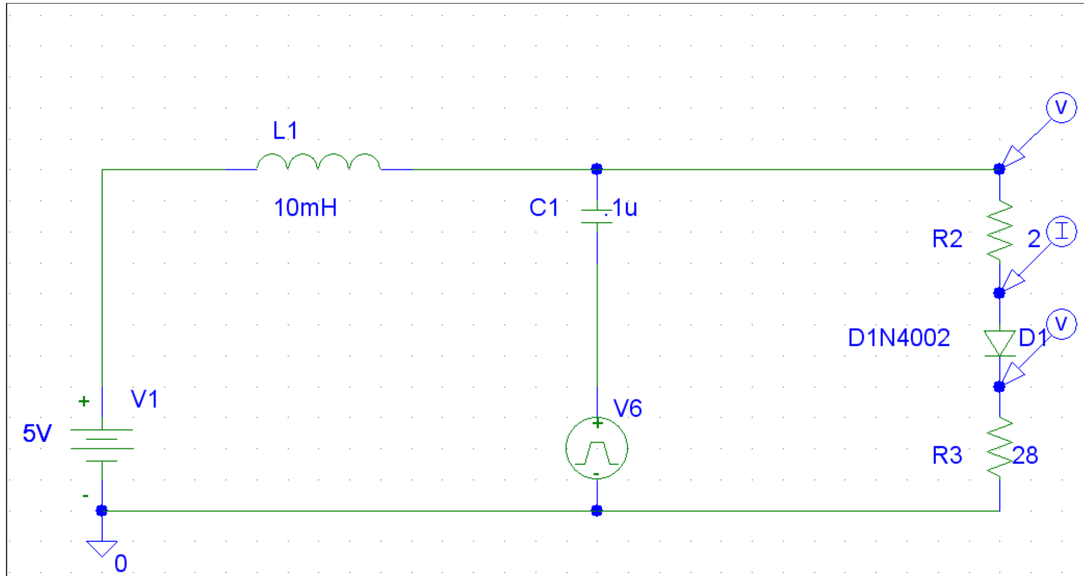

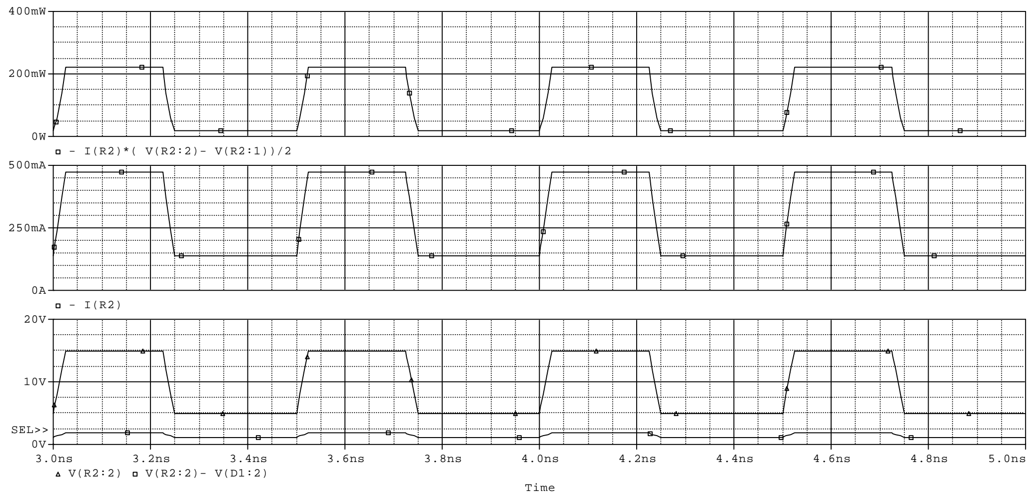

Figure 4.7. PSpice simulation of bias tee drive circuit and laser load.

Figure 4.7 shows the bias tee drive circuit with DC input, left, and RF input, center. Because of difficulty in simulating a triangular taper, the output impedance of the RF source was simply set to the total load impedance. The laser is represented by the 2 Ω resistor and the diode. It was found in simulation that a 5 V DC bias input to the bias tee worked better than 8.3 V for setting the lower laser current to ~140 mA. The first plot shows the possible light power emitted from the laser, calculated by dividing the power dissipated by the 2 Ω resistor by two, to approximate the actual power use of a diode laser. The emitted power has an on-state value of approximately 210 mW. The second plot shows the current through the laser diode, alternating between 140 mW and 470 mW, close to what was calculated, after the change in DC bias mentioned above. The final plot has two traces. The upper trace is the output voltage of the bias tee and the lower trace is the voltage across the laser diode.

4.5 LASER FOCUSING

The goal of the optical system that will focus the laser is to create a spot of at least 286 μm^2 on the photoswitch. Converging lenses are needed, since the full width at half magnitude divergences, vertical and horizontal, are $D_{vert} < 38^{\circ}$ and $D_{horiz} < 8^{\circ}$. A method of trial and error of different lens systems was used to find the best system. To calculate the effects of lens systems, the systems were converted to their ABCD matrices (see Chapter 2) and the following formula, the Gaussian ABCD law was used [2]:

$$q_2 = \frac{Aq_1 + B}{Cq_1 + D} \tag{4.4}$$

where

$$\frac{1}{q} = \frac{1}{R} - j\frac{\lambda}{\pi w^2} \tag{4.5}$$

and R is the radius of curvature of the beam (the radius of the circle that the wavefront makes, e.g. $R = \infty$ for a flat wavefront), w is the beam waist (the transverse distance from the center of the beam to a 1/e intensity point), and λ is the wavelength of the light. Note that the beam considered here is not circular in cross section, but is an elliptical Gaussian beam. The Gaussian ABCD law applies equally well to circular and elliptical Gaussian beams with the two ellipse axes taken one at a time, and elliptical Gaussian beams have the same location along the beam of the component minimum beam waists provided the far-field approximation is valid, i.e. minimum beam waist $w_0 \ll z$, the distance along the beam until another minimum beam waist is encountered (after focusing), and this criterion is met by the system considered here [18].

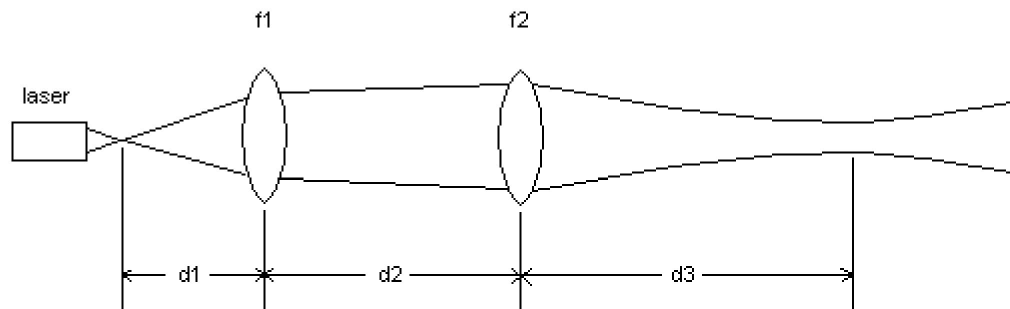

Figure 4.8. Laser focusing reference diagram.

The diagram of the system is shown in figure 4.8. f_1 and f_2 are the focal lengths of the lenses, d_1 is the distance from the laser to the first lens, d_2 is the distance between the two lenses, and d_3 is the distance from the second lens to the minimum beam waist following that lens. It was found that two lenses are best, since, if only one lens is used,

the focal length of the lens needs to be impractically small. The components of the ABCD matrix for this system are:

$$A = 1 - \frac{d_2}{f_1} - \frac{d_3}{f_1} - \frac{d_3}{f_2} + \frac{d_2 d_3}{f_1 f_2}$$

$$B = d_1 + d_2 + d_3 - \frac{d_1 d_2}{f_1} - \frac{d_1 d_3}{f_1} - \frac{d_1 d_3}{f_2} - \frac{d_2 d_3}{f_2} + \frac{d_1 d_2 d_3}{f_1 f_2}$$

$$C = -\frac{1}{f_1} - \frac{1}{f_2} + \frac{d_2}{f_1 f_2} \tag{4.6}$$

$$D = 1 - \frac{d_1}{f_1} - \frac{d_1}{f_2} - \frac{d_2}{f_2} + \frac{d_1 d_2}{f_1 f_2}$$

The beam waists (vertical and horizontal) at the laser can be assumed to be minimum beam waists, which are each obtained from the beam divergence as follows:

$$w_0 = \frac{1.18\,\lambda_0}{\pi\, n\, D} \tag{4.7}$$

where λ_0 is the free-space wavelength of the light, n is the refractive index of the medium (n = 1), and D is in radians now. w for q_1 in equations 4.4 and 4.5 is then 470 nm when considering the vertical dimension and 2 μm when considering the horizontal direction.

Considerations when choosing the focal lengths and distances are to make sure that the beam waists fall within the apertures of the lenses so no light is lost (lenses available in the lab are about 2 cm in diameter), that the focal lengths are from the set of available lenses in the lab, that d_2 is an integral number of optical table mounting hole spacings (1 inch), and that at the minimum beam waist following the second lens, where the photoswitch will be placed, the area of the spot is above 286 μm^2 so the photoswitch can't be damaged. The results of many trial and error calculations to determine the ideal arrangement are:

$f_1 = 25.4$ mm

$f_2 = 38.1$ mm

$$d_1 = 11.1 \text{ mm} \quad (4.8)$$

$$d_2 = 25.4 \text{ mm}$$

$$d_3 = 24.5 \text{ cm}$$

$$\text{area of spot} = 298\ \mu\text{m}^2$$

Note that the FWHM divergences of the laser are quoted as less than a certain number of degrees and these maximum angles were used in the above calculations. This is not a problem since, as the angles are decreased, the spot size increases. The largest dimension of the spot is two times the horizontal waist or 38 μm, about half the size of the photoswitch.

Since dimensions in the lab may not be exactly what was arrived at here (particularly the distance between the two lenses, which will be affected by the mounting and finite size of the lenses), what is prescribed is to adjust the location of the laser around 10 mm until the minimum beam waist occurs at 24.5 cm from the second lens. Then the spot size will be right.

CHAPTER 5

MICROSTRIP CLASS E AMPLIFIER

5.1 CLASS E AMPLIFIERS

As mentioned in chapter 1, the class E amplifier is the most efficient type of amplifier for the generation of constant-frequency sinusoids among the many types of amplifiers considered. See reference [1] for more comprehensive theory on class E amplifiers. Figure 5.1 shows the classical lumped-element class E amplifier. The class E amplifier is a switching amplifier with the ideal active device being a switch with zero on-resistance and infinite off-resistance. In reality, there are losses associated with nonideal switching, especially in the on-off and off-on transitions. The class E amplifier reduces these losses by having the switch voltage V_s drop to zero immediately before the switch closes and the switch current I_s drop to zero immediately before the switch opens (fig. 5.2).

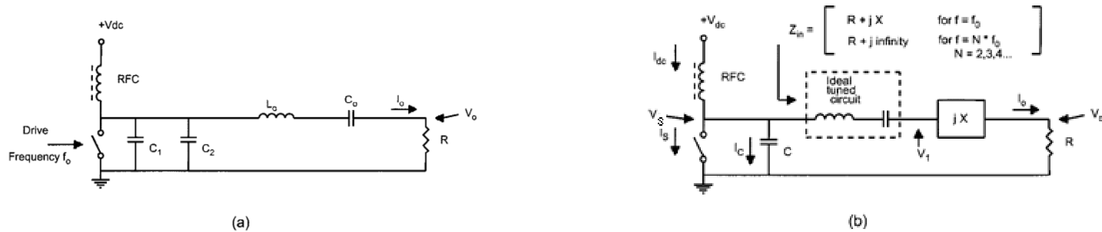

Figure 5.1. (a) Lumped-element class E amplifier. (b) equivalent circuit. [19]

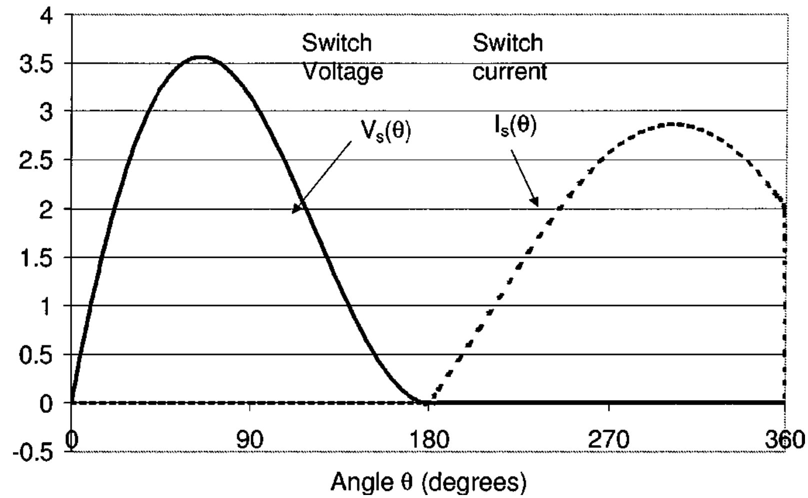

Figure 5.2. Class E switch waveforms [19].

In figure 5.1(a), the parasitic shunt capacitance of the switch is C_1 and parasitic series inductance is neglected. In the equivalent circuit, (b), $C = C_1 + C_2$ and the series reactive elements are equivalent. The RF choke (RFC) feeding the switch is assumed infinite in inductance to give a constant current and the output filter is assumed to pass the fundamental and no harmonics.

5.2 LUMPED-ELEMENT DESIGN

Below are the design equations [20] of a class E amplifier with 50% duty cycle and zero voltage and zero voltage derivative at the switch-on instant. Setting $V_{dc} = 1$ and $P_o = 1$ and using a 50% duty cycle gives figure 5.2.

$$\text{Output Power: } P_o = \frac{V_{dc}^2}{R_{dc}} \tag{5.1}$$

$$\text{Equivalent dc resistance: } R_{dc} = 1.7337\ R \tag{5.2}$$

$$\text{Shunt susceptance: } B = \omega C = \frac{1}{5.4466\ R} \tag{5.3}$$

Load angle: $\psi = 49.052°$ (inductive) (5.4)

Load-network impedance: $Z = R + jX$ (5.5)

where: $X = R \tan\psi = 1.152\ R$ (5.6)

Peak switch voltage: $V_{s\,max} = 3.56\ V_{dc}$ (5.7)

Peak switch current: $I_{s\,max} = 2.84\ I_{dc}$ (5.8)

$V_{dc} = R_{dc} I_{dc}$ (5.9)

The photodetector, a PIN photodiode, obtained for use as the photoswitch, has a capacitance of C = 4 pF and a practical $I_{s\,max}$ of 8 mA. From eqs. 5.1 – 5.9,

$$V_{s\,max} = \frac{1.2701 \cdot 10^8}{f} \qquad (5.10)$$

where f is frequency. The amplifier to power the laser operates in the frequency spectrum from 0.5 to 2 GHz, so reasonable possibilities for the operating frequency and harmonics at the input of the class E amplifier are 2 GHz with no harmonics, 1 GHz with one harmonic, and 0.5 GHz with 2 harmonics. $V_{s\,max}$ would be 64 mV, 127 mV, and 254 mV, respectively. A choice of 0.5 GHz was made to keep the most harmonic content and not too low a power (voltage). The MSM photodiode photoswitch, which was not successfully fabricated, would have had a lower capacitance, leaving more room for output power, but the purchased PIN photodiode should work.

With the frequency set to 0.5 GHz, parameters of the class E amplifier can be determined from equations 5.1 through 5.9:

$f = 0.5$ GHz

$P_o = 201\ \mu W$

$R = 14.6105\ \Omega$

$R_{dc} = 25.3302\ \Omega$

$$C = 4\ \text{pF} \tag{5.11}$$

$V_{s\,max} = 254.024$ mV

$V_{dc} = 71.355$ mV

$I_{s\,max} = 8$ mA

$I_{dc} = 2.8169$ mA

The switch has to provide an average of 2 I_{dc} for the positive half-cycle (on-state) or 5.634 mA. Given that the responsivity of the photodetector at 830 nm is 0.155 A/W, the light power in the on-state must be, at a minimum, $P_{light} = 36.348$ mW.

In [19], it was found that a higher load angle than theoretically predicted worked better, so taking an intermediate value (between that of [19] and the theoretical value) of $\psi = 54°$ gives

$$L_X = \frac{R \tan\psi}{\omega} = 6.40108\ \text{nH}\,. \tag{5.12}$$

The load resistance has been calculated to be R = 14.6105 Ω, but the actual load is a standard 50 Ω, so an impedance transformation is necessary (fig. 5.3).

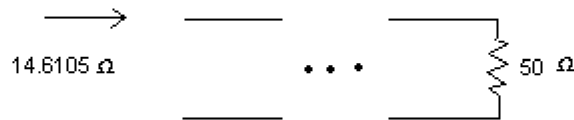

Figure 5.3. Necessary impedance transformation.

A two-stage impedance transformer will be used [21], so, to divide the impedance transformation equally between the stages, (14.6105 Ω) x^2 = 50 Ω and the intermediate impedance is (14.6105 Ω) x ≈ 27 Ω. For the first stage (stages labeled right to left), see figure 5.4.

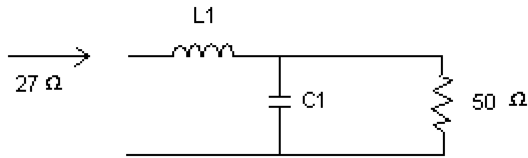

Figure 5.4. First impedance transformation stage.

The equation for this stage is:

$$27\,\Omega = j\omega L_1 + \frac{\frac{50\Omega}{j\omega C_1}}{\frac{1}{j\omega C_1} + 50\Omega} \qquad (5.13)$$

giving $C_1 = 5.87573$ pF and $L_1 = 7.93224$ nH. Similar calculations for stage 2, the stage going into stage 1, give $C_2 = 10.8563$ pF and $L_2 = 4.28262$ nH. Combining L_X and L_2, the resulting class E amplifier, without harmonic suppression yet, is shown in figure 5.5.

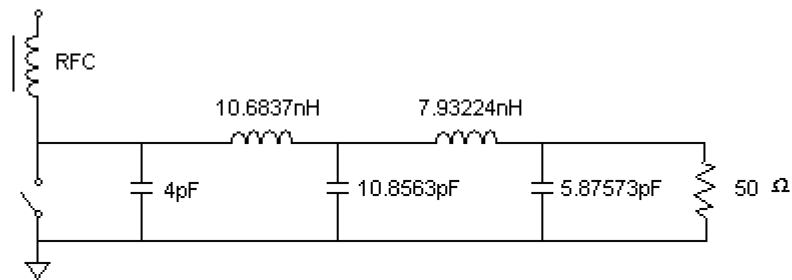

Figure 5.5. Lumped-element class E amplifier without harmonic suppression.

Before moving on to the microstrip realization of the class E amplifier, a PSpice simulation of the circuit in figure 5.5 will be performed.

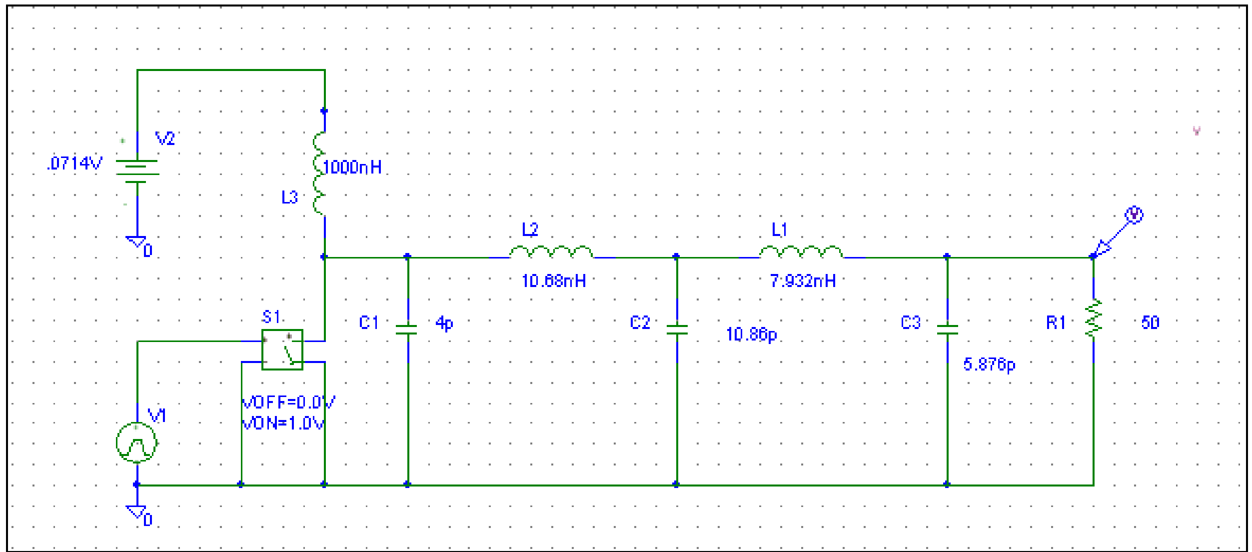

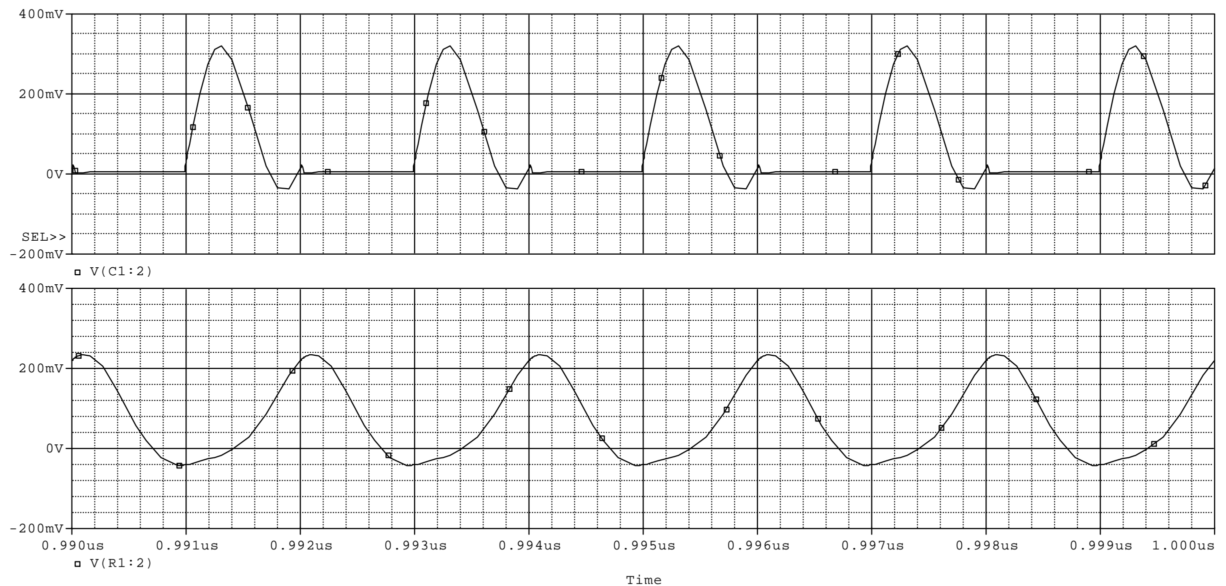

Figure 5.6. PSpice simulation of class E amplifier without harmonic suppression.

The first plot in figure 5.6 is the voltage across the switch and the second plot is the load voltage. The DC current and voltage (at the top of the RF choke) were simulated to be I_{dc} = 4.21 mA and V_{dc} = 71.4 mV giving an input dc power of P_{dc} = 300 µA. The peak-to-peak value of the load voltage is 240 mV. Using the equation for the power of a sinusoidal voltage across 50 Ω as an approximation with that peak-to-peak value gives:

$$P_{RFout} = \frac{(0.5\ V_{p-p,out})^2}{2\ (50\ \Omega)} = 144\ \mu W. \quad (5.14)$$

The simulated anode efficiency of the class E amplifier is then:

$$\eta = \frac{P_{RFout}}{P_{DC}} = 48\%. \quad (5.15)$$

Note that the load voltage is not centered at zero, so the output power is actually higher than the calculated value, with some DC power. Even if a capacitor is placed between the load and the rest of the amplifier, though, the average load voltage is still far from zero, so it is assumed that PSpice does not simulate the circuit 100% correctly.

Finally, PSpice will be used again to simulate the class E amplifier, but this time with harmonic suppression. Note that the method to suppress harmonics in the PSpice simulation, an LC filter, is not the same as that used in the microstrip realization (see the next section), but the simulation will give some idea of what to expect when harmonic suppression is added.

.

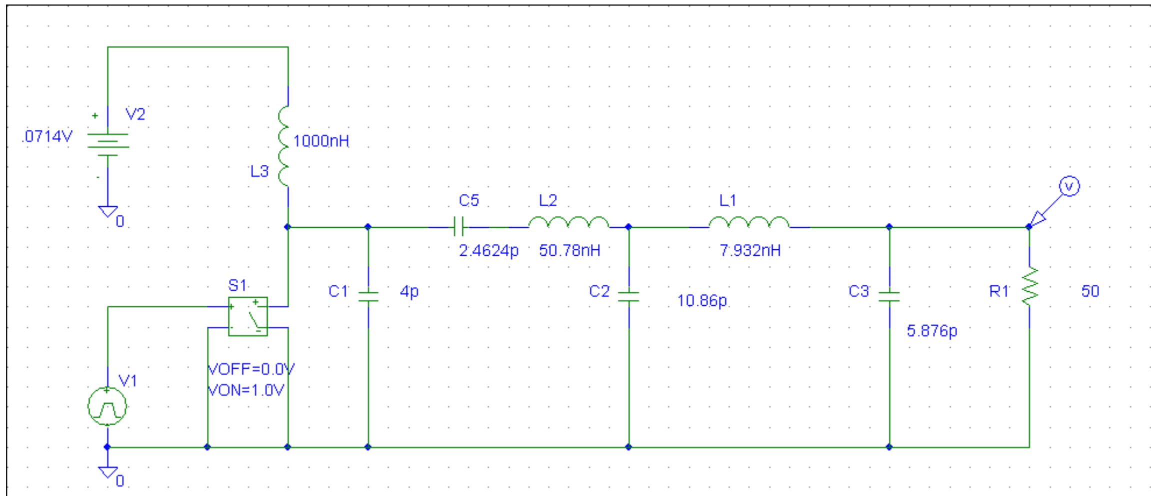

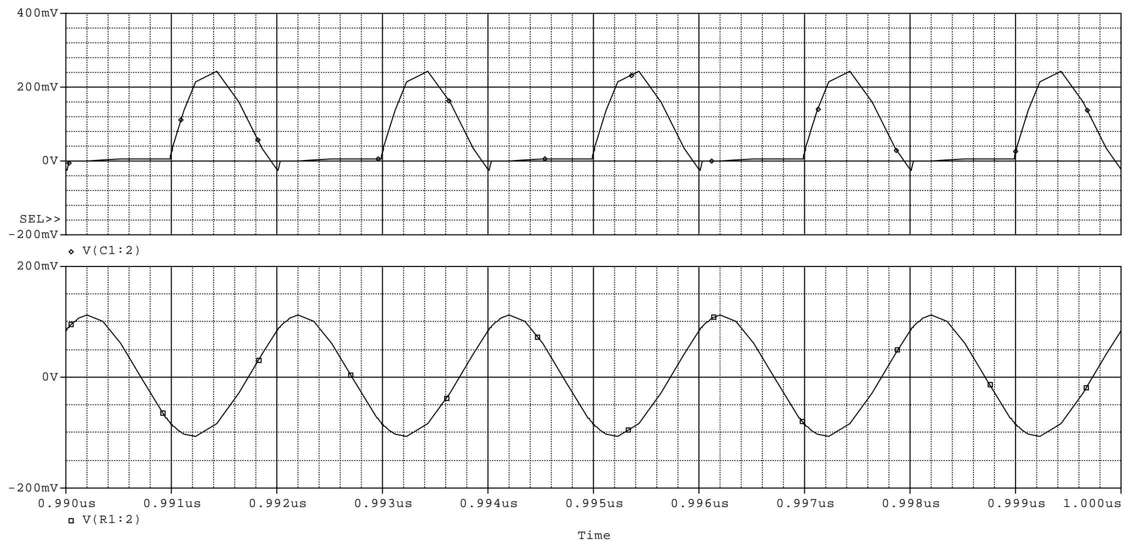

Figure 5.7. PSpice simulation of class E amplifier with harmonic suppression.

The PSpice simulation is shown in figure 5.7. Again, the first plot is the voltage across the switch and the second plot is the load voltage. Note that the load voltage is now approximately sinusoidal, as desired. By a similar calculation to the one above for the amplifier without harmonic suppression, the anode efficiency is found to be 92%, a marked improvement.

5.3 MICROSTRIP REALIZATION

A microstrip transmission line realization of the class E amplifier was decided upon. Lumped element realization is possible at 0.5 GHz with a monolithic microwave integrated circuit (MMIC), but this technology was unavailable. Furthermore, as the amplifier is scaled up to 10 GHz, the target frequency for the application of the present research, MMIC implementation becomes more difficult and its main advantage – small size – becomes less of an issue (the higher the frequency is, the smaller a microstrip circuit is).

It is necessary, then, to translate the circuit in figure 5.5 into a microstrip circuit. The series inductances can be realized by short sections, less than $\lambda/8$ where λ is the wavelength of the 0.5 GHz signal in the transmission line [19], of high impedance. The shunt capacitances can be realized by lower impedance open-circuit stubs. See figure 5.8.

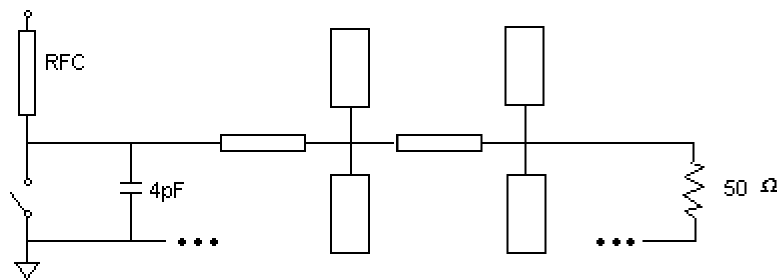

Figure 5.8. Microstrip realization of class E amplifier.

Notice in figure 5.8 that each capacitance is realized by two open-circuit stubs (up and down in the figure). This leads us to an additional feature that can be built into the

microstrip circuit: harmonic suppression. If the stubs are set to lengths of $\lambda/4$ where λ are the wavelengths of 1.0, 1.5, 2.0, and 2.5 GHz signals, then these harmonics see zero impedance and are suppressed from appearing at the load. The stubs then have two functions: to appear as shunt capacitance and to perform the same function as the LC filter ("ideal tuned circuit") in figure 5.1(b).

The method of calculation of the dimensions of the open-circuit stubs will now be covered [19]. First, an initial guess at what their characteristic impedances, Z_{0A} for C_2 (the left two stubs) and Z_{0B} for C_1 (the right two stubs), is made. Then, using the formulas in Appendix A, the impedances are translated to microstrip widths, one for the left side and one for the right, given a frequency of 0.5 GHz and the available circuit board's dielectric constant of 2.5 and thickness of 1.5748 mm. Appendix A is again used to find the effective dielectric constants, ε_{eff}, at 0.5, 1.0, and 1.5 GHz for the left stubs and 0.5, 2.0, and 2.5 GHz for the right stubs given their widths. Lengths of the four stubs, $l_{1.0GHz}$, $l_{1.5GHz}$ on the left and $l_{2.0GHz}$, $l_{2.5GHz}$ on the right, are then calculated by, for example,

$$l_{1.0GHz} = \frac{\lambda_{0,1.0GHz}}{4\sqrt{\varepsilon_{eff,1.0GHz}}} \tag{5.16}$$

where $\lambda_{0,1.0GHz}$ is the free space wavelength of a 1.0 GHz signal (i.e., 30 cm). This takes care of harmonic suppression. Then the electrical lengths, in degrees, $EL_{1.0}$, $EL_{1.5}$, $EL_{2.0}$, and $EL_{2.5}$, representing the fraction, in degrees, of a wavelength of a 0.5 GHz signal contained, are calculated for these stubs, e.g.,

$$EL_{1.0} = \frac{360°\, l_{1.0GHz}\sqrt{\varepsilon_{eff,0.5GHzA}}}{\lambda_{0,0.5GHz}} \tag{5.17}$$

where $\varepsilon_{eff,0.5GHzA}$ refers to the effective dielectric constant at 0.5 GHz for the left-side stubs. $EL_{1.0}$ is, for example, a little less than 45° (approximately half of the 90° at the

suppressed frequency). Now the formula for the capacitance of an open-circuit stub is used [19]:

$$C = \frac{EL}{360° Z_0 f} \quad . \tag{5.18}$$

Setting the characteristic impedances of the left-side stubs equal (= Z_{0A}, but the updated value) and introducing an intermediate variable, C_A, for the capacitance of just the upper stub,

$$Z_{0A} = \frac{EL_{1.0}}{360°\, f\, C_A} = \frac{EL_{1.5}}{360°\, f\, (C_2 - C_A)} \tag{5.19}$$

where C_2 is obtained from the impedance transformer in Section 5.2. This gives a result for Z_{0A}. Z_{0B} is calculated by a similar method. Then, the above steps are repeated with the new characteristic impedances and the process is iterated by hand until all values converge. At the end, the widths of the microstrips (left and right) are calculated from the characteristic impedances (Appendix A). The final results are:

$$\begin{aligned} w_{left} &= 6.56972 \text{ mm} \\ l_{1.0GHz} &= 51.128 \text{ mm} \\ l_{1.5GHz} &= 34.051 \text{ mm} \\ w_{right} &= 6.61093 \text{ mm} \\ l_{2.0GHz} &= 25.504 \text{ mm} \\ l_{2.5GHz} &= 20.379 \text{ mm} \end{aligned} \tag{5.20}$$

Now, the inductive widths and lengths are determined. $Z_0 = 85\ \Omega$ was chosen for all inductances, as in [19]. Also as in [19], EL = 35° was chosen for the RF choke. The formulas for the inductance of a short transmission line section are [19]:

$$L = \frac{Z_0\, EL}{360°\, f} \qquad l = \frac{EL\, \lambda_0}{360° \sqrt{\varepsilon_{eff}}} \tag{5.21}$$

Here are the results (using Appendix A):

$$w = 1.78389 \text{ mm}$$
$$l_{RFC} = 41.463 \text{ mm}$$
$$l_{L,left} = 26.802 \text{ mm} \qquad (5.22)$$
$$l_{L,right} = 19.9 \text{ mm}$$

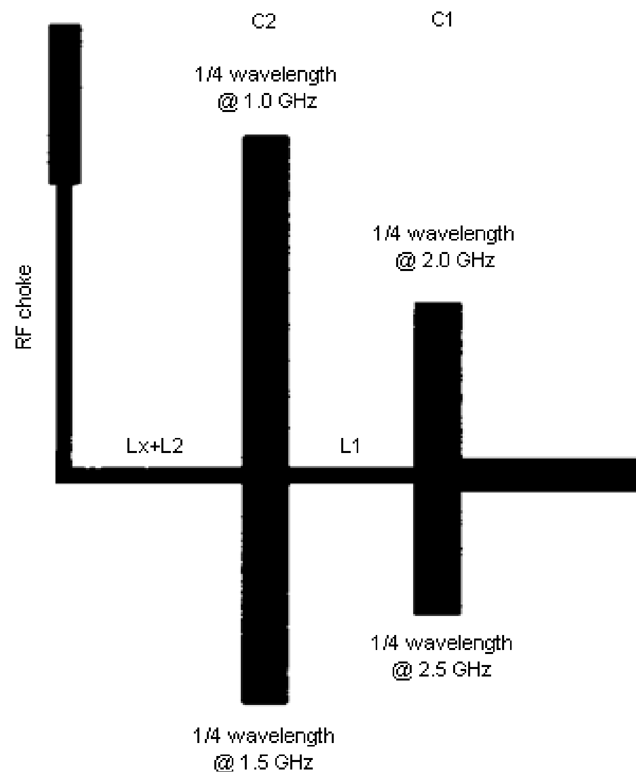

Figure 5.9. Microstrip class E amplifier

The resulting microstrip class E amplifier is shown in figure 5.9 (approximately actual size). As with any microstrip circuit, this circuit involves a metal layer (e.g., in the pattern shown in fig. 5.9) on the top surface of a dielectric board, with a metal ground plane on the bottom surface of the board. In the circuit shown, the voltage source should

be connected to the upper left line, the positive-voltage end of the photodiode (diode cathode) should be connected to the left end of the horizontal transmission line, and the load (an oscilloscope in this case) should be connected to the right end. The widths of the upper left connection and the right connection are equal (4.4751 mm) since they have a 50 Ω characteristic impedance. The diode anode should be connected to the ground plane underneath as should all of the ground terminals of everything mentioned.

CHAPTER 6

EXPERIMENTAL SET-UP, RESULTS, AND CONCLUSIONS

6.1 FIRST EXPERIMENTAL SET-UP

This section is primarily to familiarize future researchers with the equipment purchased so they can duplicate the results here. Figure 4.1(b) is reproduced as figure 6.1. It shows the excitation system (everything leading up to, but not including the photoswitch).

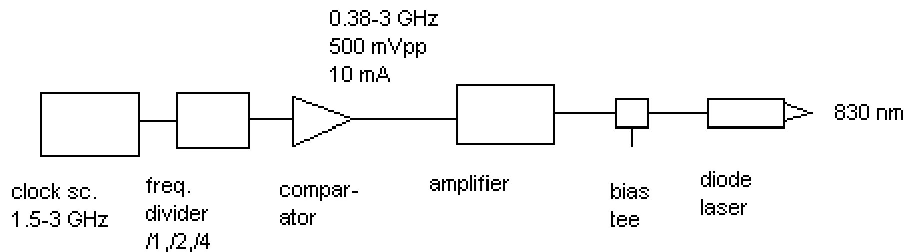

Figure 6.1. Excitation system.

First of all, the clock source (Pulse Research Labs PRL-176AN) should be set to 2 GHz and one output should be connected as the input to the frequency divider (PRL-257-2). The complementary output to this output should be terminated to 50 Ω through a capacitor (taken care of by a PRL-ACT50). Capacitors referred to in this section are simply for DC blocking and should act as a short to the RF signal, e.g. 0.1 μF would

work for all capacitances mentioned. The clock source and frequency divider both have power supplies ("AC adaptors") that came with them.

Next, the frequency divider should have a divide by 2 output run to the "VP" RF input of the Analog Devices comparator board through a capacitively coupled 20 dB attenuator (PRL-ACX-20dB). The associated complementary output should be run through the same type of attenuator to the trigger input of the oscilloscope. Note that the *measured signal* input to the oscilloscope must always be between -2 and 2 V! Use of attenuators and a capacitor is often necessary.

Next, we consider the connections to the comparator board. The following inputs should be set to ground: VTP_F, VEE, CGND, the two GND PLANE inputs, and VTN_F. The following inputs should be set at 5 V: VCCO, VTT, and VCCI. The following RF inputs should be grounded (shorted, e.g., with a PRL-FTR-0): VN and LEB. The RF input "LE" should be put at 5 V (DC). Finally, the output QB should be run through a capacitor and attenuators to the input of the RF amplifier (Phase One Microwave SP02-3233). The attenuation depends on the desired voltage swing at the output of the amplifier. Since the comparator produces 500 mV peak to peak and the amplifier has a gain of 29 dB, 5 dB of attenuation should be used for 8 V of swing, 3 dB of attenuation for 10 V of swing, and no attenuation for 13 V of swing. The RF amplifier has a dedicated 15 V power supply.

Next, a bias tee should be used to add voltage to the RF output of the amplifier. The DC input to the bias tee should be set at 4 V. This needs to be done before connecting the output of the bias tee to the input of the laser because the maximum

reverse voltage of the laser is 3 V. The connection from the output of the bias tee to the laser board can now be made and then the amplifier can be powered up.

Now, the laser-photodetector pair can be aligned. A 1 V voltage source with a capacitor across it can be run through 50 Ω in series with the detector, with the other side of the detector run to the oscilloscope. The detector is hooked up backwards if there is a constant nonzero current running through it. Two large, low focal length (thick) lenses should be placed next to each other with the detector on an x-y-z positioning stage approximately 25 cm away from one of them. The laser should be placed at the other side and its location and direction should be adjusted until the spot is minimal and approximately over the active area of the photodetector. All four elements of the optical system should be in as straight a line as possible. The positioning stage should be moved around until a signal is picked up. The current through the detector needs to be kept below 10 mA to avoid damaging it. The bias tee DC voltage should be adjusted to get 8 mA peak current out of the photodetector, but it's value should never fall below 4 V for an RF input to the bias tee of ≤13 V, or the laser might be damaged.

All that remains is to unhook the photodetector and hook it up to the class E amplifier board and measure the output.

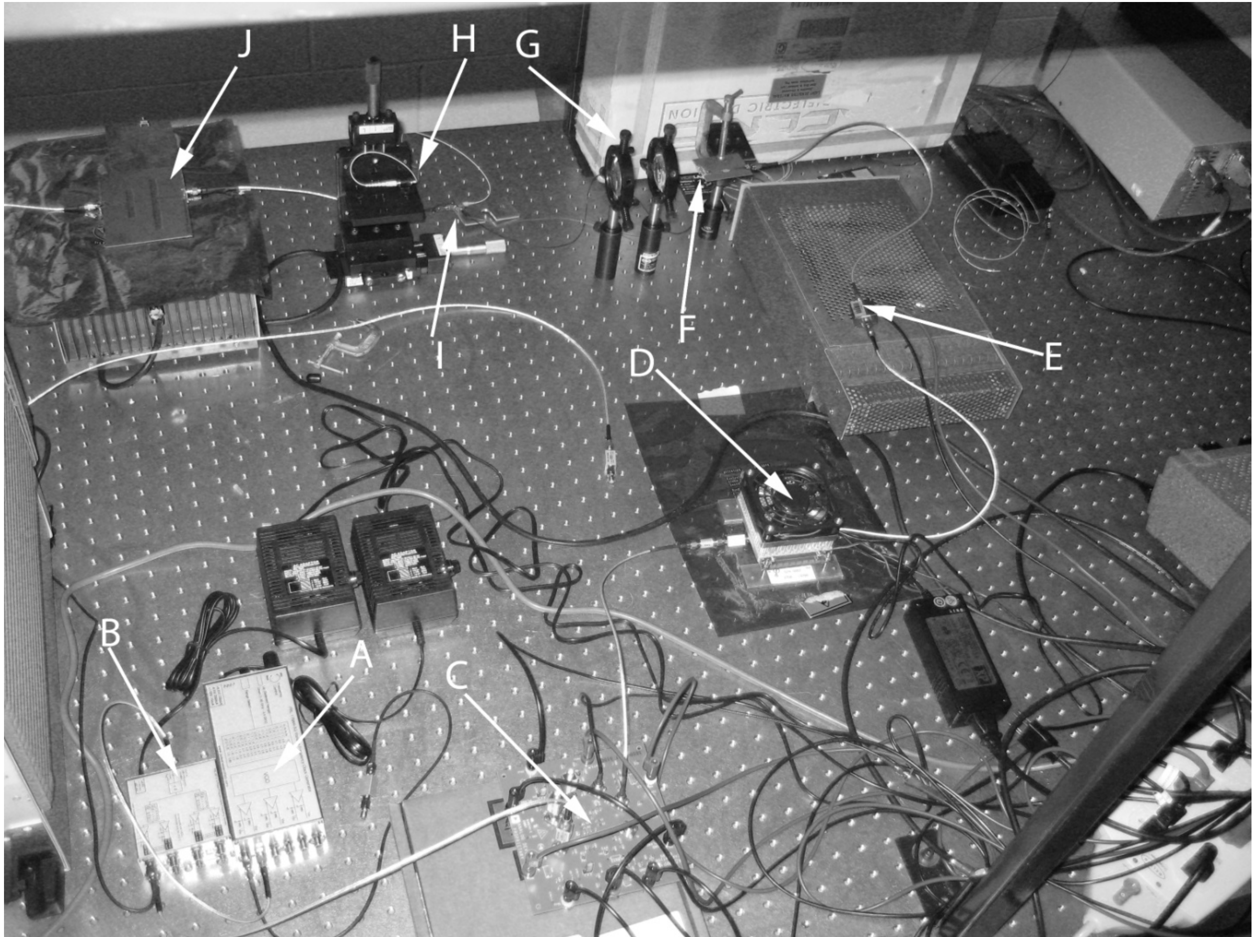

Figure 6.2. Electrically modulated laser system.

Figure 6.2 shows the electrically modulated laser system. A is the clock source; B is the frequency divider; C is the comparator; D is the RF amplifier; E is the bias tee; F is the laser; G is the two-lens optical system; H is the input for the photodetector on an XYZ translation stage; I is the photodetector; and J is the class E amplifier.

6.2 FIRST RESULTS

The methods of section 6.1 were applied using the ThorLabs FGA04 photodiode, purchased in place of the unsuccessfully fabricated photoswitch. The attempt to get a square wave varying between 0 and 8 mA through the photodiode was unsuccessful. This is attributed to the low voltage placed across the photodiode, as required by the class E amplifier design. It was hoped that the photodiode would behave at a fraction of a volt the same way, approximately, as it behaves at 5 V, the only voltage value referenced in the datasheet for the photodiode. This was not the case and the current through the photodiode remained essentially constant when a square wave light intensity was applied to it. A change of experimental set-up was then made. A 1550 nm laser with an electrooptic modulator was used in place of the electrically-modulated laser setup originally chosen. See section 6.3 for a similar experimental setup. 1550 nm is acceptable because the purchased photodiode operates well at this wavelength, unlike the original GaAs photoswitch that was unsuccessfully fabricated. When the photodiode was placed in the class E amplifier circuit, the best results obtained were as shown in figure 6.3.

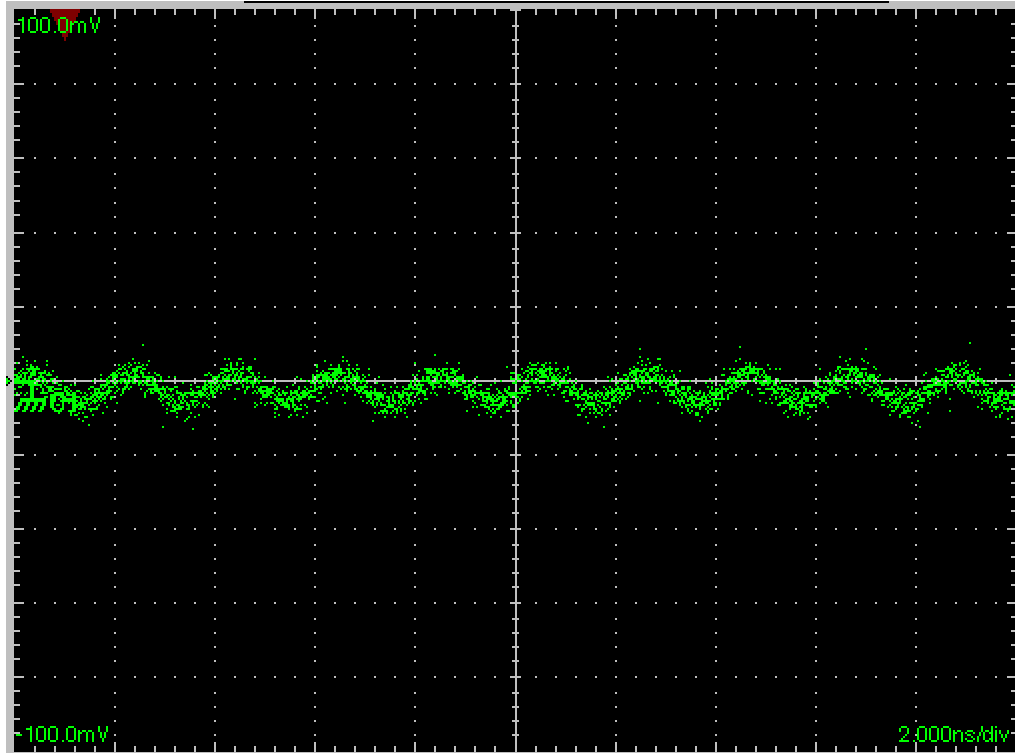

Figure 6.3. Class E amplifier output.

Figure 6.3 represents the output voltage of the class E amplifier (across a 50 Ω load) with zero volts applied to the dc input of the amplifier and a zero to 5.4 mW square wave of light applied to the photodiode. Adjusting the light intensity higher or lower reduced the magnitude of the output and adjusting the dc voltage higher simply shifted the output up by a dc voltage. The resulting output voltage is 10 mV peak-to-peak, subtracting the noise. This means that P_{RFout} is 0.25 μW with a P_{RFin} of 2.7 μW.

$$\eta = \frac{P_{RFout}}{P_{DC}} \tag{6.1}$$

$$PAE = \frac{P_{RFout} - P_{RFin}}{P_{DC}} \tag{6.2}$$

The results, then, correspond to an infinite anode efficiency and a negative infinity power added efficiency, since the denominator in both calculations is the dc input power, which is zero.

Clearly, these are not the desired results. A new experimental setup was necessary to obtain more and better data. A switch was made to a different photodiode, the Discovery Semiconductors DSC 50S, since this diode was available from a previous experiment and it was known to operate at up to 2 GHz well. The disadvantage to this photodiode, though, is that it cannot be used as a photoswitch, since the positive input to the photodiode cannot take an RF signal. The approach taken, then, was to remove the dc voltage input to the class E amplifier and insert the output (negative input or anode, since the diode is reverse biased) of the photodiode as an input to the class E amplifier where the photoswitch would be. See figure 6.4.

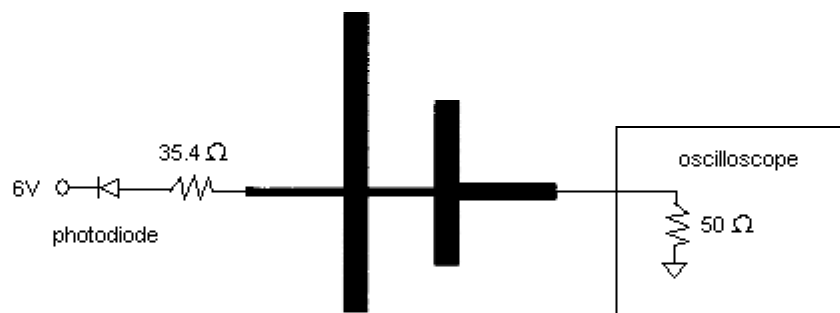

Figure 6.4. Altered, final class E amplifier setup.

Notice that the input dc voltage line (upper left) of the class E amplifier has been removed. The 35.4 Ω resistor is needed because the impedance transformation of the

designed class E amplifier gives a 14.6 Ω input impedance. The details of the laser circuit driving the photodiode are presented in the next section.

6.3 FINAL EXPERIMENTAL SET-UP

This section is, as with section 6.1, meant primarily as a resource to future researchers for use of the laboratory equipment. The laser circuit driving the photodiode is shown in figure 6.5.

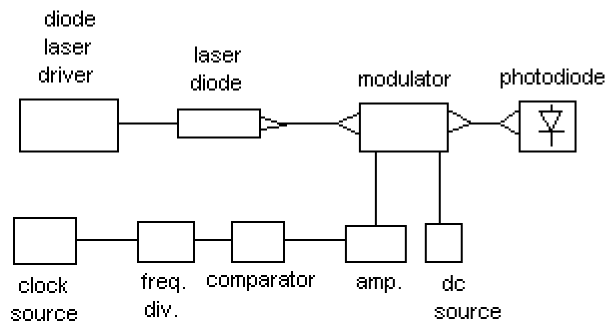

Figure 6.5. Final laser circuit.

The clock source, frequency divider, comparator and amplifier are set up as in section 6.1, with a 3 dB attenuator and a capacitor between the comparator and amplifier. The dc source is set to 4.5 V for the best square wave out of the modulator. The diode laser driver is set to provide 300 mA for the laser diode. The laser diode and modulator are connected by a polarization-maintaining optical fiber and the modulator and photodiode are connected by a standard optical fiber.

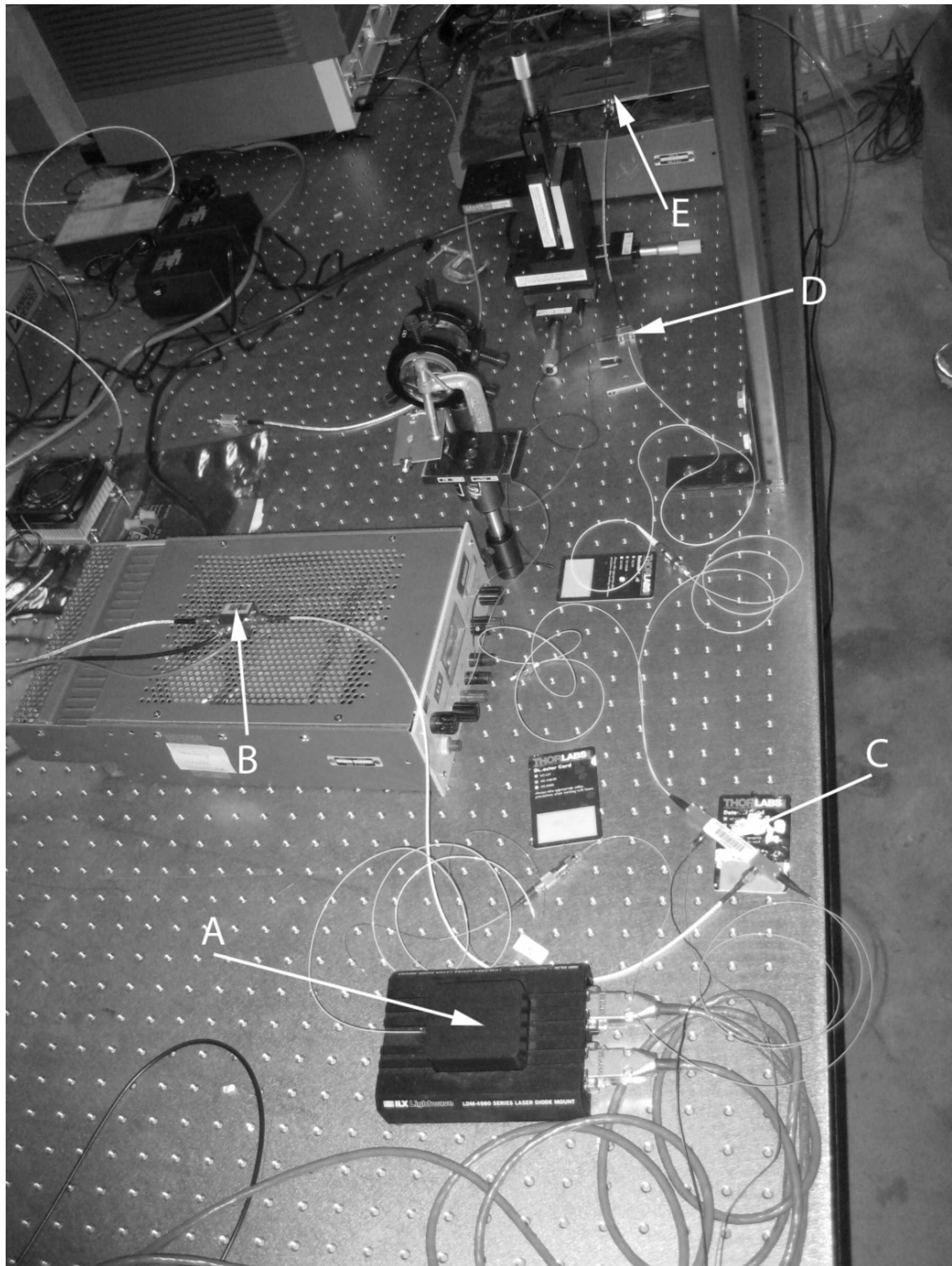

Figure 6.6. Optically modulated laser system.

Figure 6.6 shows the optically modulated laser system. A is the 1550 nm laser diode; B is the bias tee with the same input machinery as in figure 6.2; C is the EO modulator; D is the photodiode; and E is the class E amplifier/filter.

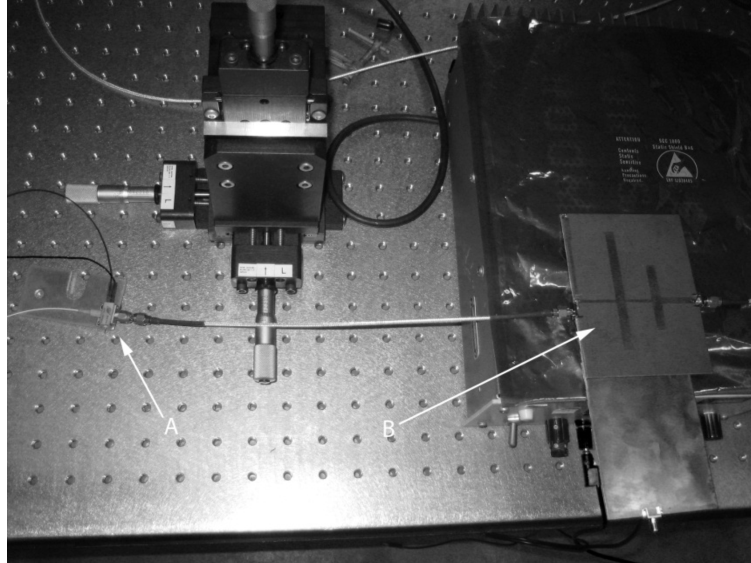

Figure 6.7. photodiode (A) and filter (B).

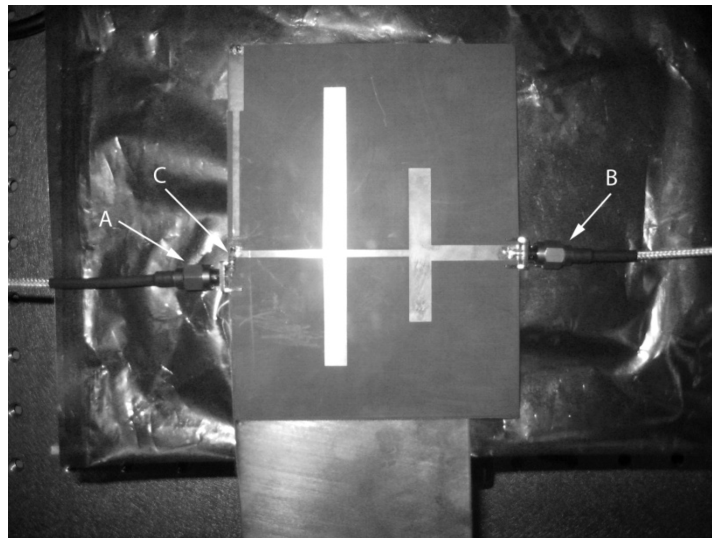

Figure 6.8. Filter derived from class E amplifier.

Figures 6.7 and 6.8 show the photodiode and the filter derived from the class E amplifier. In figure 6.8, A is the input to the filter connected to the photodiode; B is the output of the filter connected to the oscilloscope; and C is the 35 Ω resistor. Notice just

above the resistor, where the DC voltage input and RF choke are removed from the circuit by a gap.

6.4 FINAL RESULTS

The class E amplifier circuit is reproduced in figure 6.9 with the input and output voltages labeled. These input and output voltage waveforms are presented in figures 6.10 and 6.11.

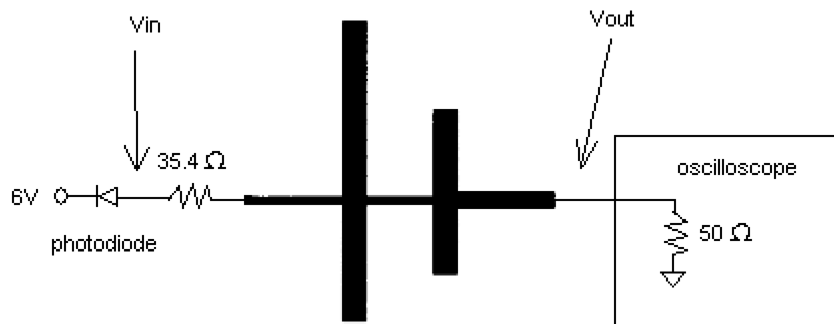

Figure 6.9. Final class E amplifier circuit.

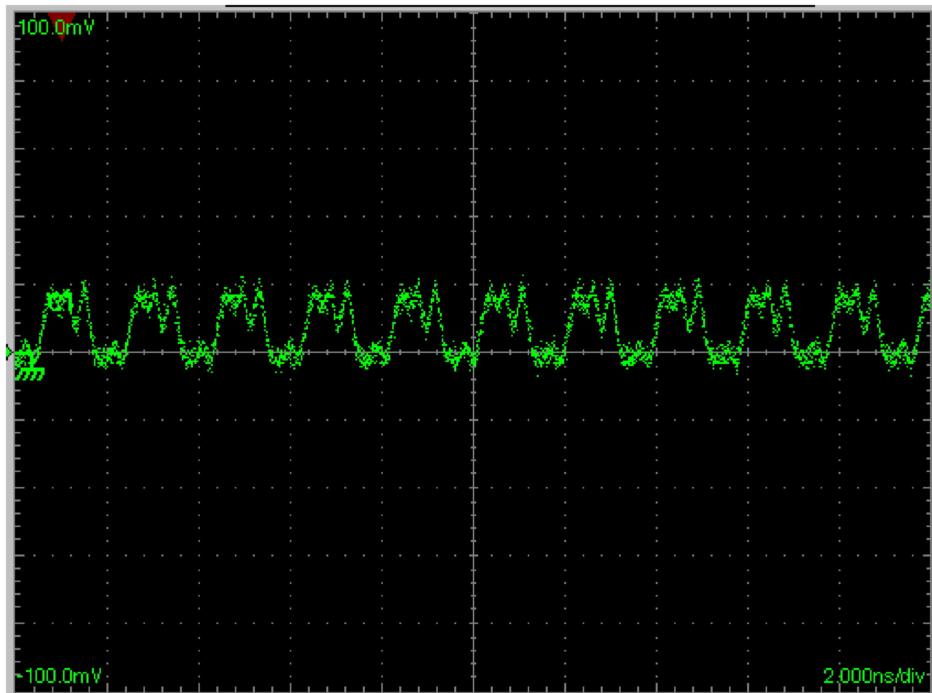

Figure 6.10. Input voltage, V_{in}.

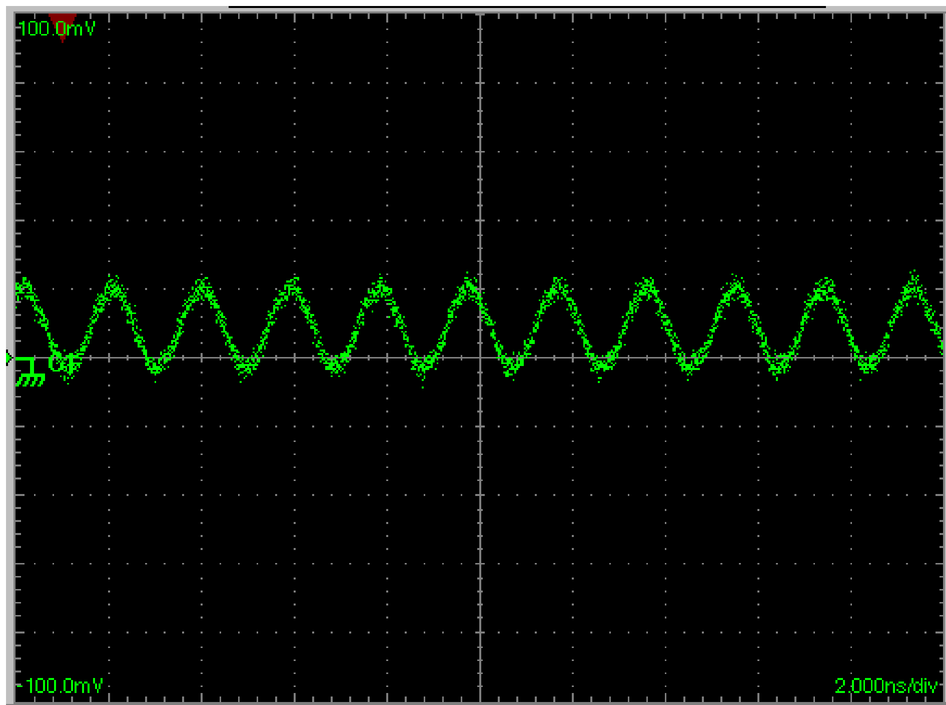

Figure 6.11. Output voltage, V_{out}.

The first thing to notice about the input and output voltages is that the class E amplifier acts as a filter as it is supposed to do and converts the distorted, approximately-square wave input into the desired sinusoidal output. It should be noted that the highest peak-to-peak output voltage was not obtained at the design frequency of 500 MHz, but occurred at 521 MHz, and data was obtained at this frequency.

Calculations of anode efficiency, η, and power-added efficiency, PAE, can now be made.

$$\eta = \frac{P_{RFout}}{P_{DC}} \tag{6.1}$$

$$PAE = \frac{P_{RFout} - P_{RFin}}{P_{DC}} \tag{6.2}$$

Again, P_{RFin} refers to the average power of the laser signal going into the photodiode. P_{DC} should be replaced by the average power of the input signal P_{in}, obtained from V_{in}. For these calculations, the average voltages are subtracted from V_{in} and V_{out}, and V_{in} is assumed to be a square wave and V_{out} is assumed sinusoidal. Additionally, the 8 mV scatter noise is subtracted from the peak-to-peak measured values of the signals, resulting in $V_{p\text{-}p,in}$ = 23.9 mV and $V_{p\text{-}p,out}$ = 25.5 mV.

$$P_{in} = \frac{(0.5\ V_{p-p,in})^2}{50\ \Omega} = 2.86\ \mu W \tag{6.3}$$

$$P_{RFout} = \frac{(0.5\ V_{p-p,out})^2}{2\ (50\ \Omega)} = 1.63\ \mu W \tag{6.4}$$

$$P_{RFin} = \frac{0.5\ V_{p-p,in}}{\text{Responsivity}\ (50\ \Omega)} = 279\ \mu W \tag{6.5}$$

where the responsivity of the photodiode in equation 6.5 is 0.8 A/W. This results in:

$$\eta = 65.4\ \% \tag{6.6}$$

$$PAE = -11.1\ \text{x}10^3\ \% \tag{6.7}$$

Clearly the PAE is undesirable, representing a much higher input light power than output RF power, but the anode efficiency is reasonable. As a matter of fact, this number represents a lower efficiency than the microstrip portion of the class E amplifier really has, since a 35.4 Ω resistor was used to match impedances correctly. The adjusted efficiency should use

$$P_{in,adj} = \frac{50\ \Omega}{50\ \Omega + 35.4\ \Omega} P_{in} = 1.67\ \mu W, \tag{6.8}$$

giving

$$\eta_{adjusted} = 97\ \%. \tag{6.9}$$

6.5 CONCLUSIONS

Because of the limitations of fabrication facilities on campus and purchased devices, this experiment has not proceeded as it was intended, but much has been learned about how to better approach the problem (see Chapter 7). The resulting efficiency of 97 % shows that the class E amplifier microstrip circuit acted as it was supposed to, to the extent that it could be tested. It was not used as a conventional class E amplifier, but more as a filter, since instead of a constant current source and a switch to ground, it had a square-wave input voltage. Power added efficiency could be increased by increasing light intensity. The quickest way to improve the results, though, would probably be to fabricate the intended photoswitch, or a better one (see Chapter 7), and redesign the microstrip class E amplifier around this photoswitch.

A notable lesson learned was that if one is using an RF signal to drive a laser and electrically modulate it, this signal probably expects a 50 Ω load, so the 1 or 2 Ω laser is

bound to receive only a small fraction of the power of the amplifier, since it must be in series with a much higher resistance. The electrically modulated system chosen in Chapter 4, then, is probably no longer the best choice. Recommendations for future work are contained in the next chapter.

CHAPTER 7

FUTURE WORK

There are a number of ways to further pursue the viability of the optically-switched class E amplifier investigated in this study aside from successfully implementing the designs here. More research can be done to achieve an implementation which comes close to the simulated anode efficiency of 80.1% and power-added efficiency of 59.3% at the simulated frequency of 10 GHz [1]. Switching to optical modulation and amplification, altering the photoswitch design, and achieving better coupling of the light into the photoswitch are all possible further research directions.

7.1 OPTICAL MODULATION AND AMPLIFICATION

First of all, to extend the frequency from 0.5 or 2 to 10 GHz, making the amplifier more applicable to radar, optical modulation of the output of the laser with an EO intensity modulator would be preferable to electrical modulation of the signal driving the laser. This is because modulating a laser electrically becomes very difficult when the frequencies move into the tens or more GHz, the harmonics making up the square wave of a 10 GHz signal. Many microwave components, such as SMA cables and connectors, are only good up to 20 GHz, insufficient for a very good square wave. Also, as mentioned at the end of the previous chapter, electrical modulation can result in much

waste of power driving the laser. Furthermore, mounting a laser without having prohibitive L/R time constants at 10 GHz and above is difficult.

As mentioned in chapter 4, frequency doubling is cumbersome and inefficient, with only 65% efficiency using 10 frequency doubling crystals. What is needed is an optical amplifier at the target wavelength of approximately 800 nm or a different switch material that would work at 1550 nm. A low-power 800 nm laser can be optically modulated to produce a low-power square wave, and then an 800 nm fiber laser (fiber amplifier) would be used to bring the signal up to the desired power. This would likely be easier to implement than an electrically-modulated system, provided the fiber laser were available. An easy fix, though, would be the use of Indium Gallium Arsenide (InGaAs) as a switch material instead of GaAs. InGaAs can be made to have high responsivity at 1550 nm. Only silicon and GaAs were considered as switch materials in this work, as was done by the previous researchers on this project, so alternative materials should be considered.

7.2 PHOTOSWITCH DESIGN

A necessary change would be of the photoswitch, itself, to more closely match the design in [1]. First of all, the spacing between the electrodes should be reduced from 1.5 to 0.5 µm for faster action. This would require better fabrication resources, especially electron beam lithography, to break the 1 µm barrier. Second, the electrodes could penetrate up to 5 absorption depths (about 5 µm) into the GaAs to bring speed up more fully without sacrificing breakdown voltage. This would also require better fabrication

resources, namely dry (plasma) etching of the GaAs for vertical walls and probably chemical vapor deposition of the metal or electroplating to fill the high aspect ratio (height over width) channels. Carbon doping could be investigated for engineering the carrier lifetime, as well, but sources for carbon doping are typically hard to obtain Russian papers.

With the reduced electrode spacing, though, the breakdown voltage is reduced, so to overcome the limited output voltage, stacked photoswitches could be used, where the cathode of one photoswitch is the anode of the next one. This is a counterintuitive design, but it should work. The drawback, however, is that n times as much optical power is required for n photoswitches in the stack, so power added efficiency is reduced.

7.3 LIGHT COUPLING

Finally, coupling of the light into the photoswitches should be addressed to achieve maximum efficiency. With better fabrication resources, perhaps the width of electrodes could be reduced, though this may not be possible given how high the aspect ratio of the electrode channels would be. The light could also be directed more into the channels. A waveguide or some sort of grating might work to direct the light around the electrodes, or a single gap might be used, as in [1], along with a cylindrical lens, though alignment would be difficult. The easiest step in increasing coupling would be the use of an anti-reflective coating (ARC). The ARC should have a refractive index of close to 1.92 as an intermediate between air and GaAs. SiO closely matches this. A thickness of

approximately 100 nm would be used to increase the transmittance into the GaAs from approximately 67% without an ARC to close to 100%.

APPENDIX A

COMPUTATION OF CHARACTERISTIC IMPEDANCE AND EFFECTIVE DIELECTRIC CONSTANT OF A MICROSTRIP TRANSMISSION LINE

A maximum relative error for Z_0 and ε_{eff} is found to be 1% for the following equations if $2 \le \varepsilon_r \le 18$, $0.1 \le w/h \le 10$, and $0 \le h/\lambda_0 \le 0.1$ [16].

$Z_0 = x_{29}$, $\varepsilon_{eff} = x_{21}$.

$x = w/h$, $y = \varepsilon_r$, $z = \frac{f}{GHz} \frac{h}{mm}$.

$x_1 = 0.03891\ y^{1.4}$, $x_2 = 0.267\ x^7$, $x_3 = 4.766 \exp(-3.228\ x^{0.641})$,

$x_4 = 0.016 + (0.0514\ y)^{4.524}$, $x_5 = (z/28.843)^{12}$, $x_6 = 22.20\ x^{1.92}$,

$x_7 = 1.206 - 0.3144 \exp(-x_1)\ (1 - \exp(-x_2)$,

$x_8 = 1 + 1.275\ (1 - \exp(-0.004625\ x_3\ y^{1.674}\ (z/18.365)^{2.745}))$,

$x_9 = 5.086\ x_4\ x_5 \exp(-x_6)\ (y\text{-}1)^6 / (\ (0.3838 + 0.386\ x_4)\ (1 + 1.2992\ x_5)\ (1 + 10(y\text{-}1)^6)\ )$,

$x_{10} = 0.00044\ y^{2.136} + 0.0184$, $x_{11} = (z/19.47)^6 / (1 + 0.0962\ (z/19.47)^6)$,

$x_{12} = 1 / (1 + 0.00245\ x^2)$, $x_{13} = 0.9408\ (x_{21})\text{\^{}}(x_8) - 0.9603$,

$x_{14} = (0.9408 - x_9)\ (x_{18})\text{\^{}}(x_8) - 0.9603$, $x_{15} = 0.707\ x_{10}\ (z/12.3)^{1.097}$,

$x_{16} = 1 + 0.0503\ y^2\ x_{11}\ (1 - \exp((-x/15)^6)$,

$x_{17} = x_7\ (1 - 1.1241\ (x_{12}/x_{16}) \exp(-0.026\ z^{1.15656} - x_{15})\ )$,

$x_{18} = (y + 1)/2 + ((y - 1)/2)(1 + 10/x)\text{\^{}}(-x19\ x20)$,

$x_{19} = 1 + (1/49) \ln(\ (x^4 + (x/52)^2) / (x^4 + 0.432)\ ) + (1/18.7) \ln(1 + (x/18.1)^3)$,

$x20 = 0.564\ (\ (y - 0.9) / (y + 3)\ )^{0.053}$, $x21 = y - (y - x_{18}) / (1 + x_{22})$,

$x_{22} = x_{23}\, x_{24}\, ((0.1844 + x_{25}\, x_{26})\, z\,)^{1.5763}$,

$x_{23} = 0.27488 + (0.6315 + 0.525 / (1 + 0.0157\, z)^{20})\, x - 0.065683\, \exp(-8.7513\, x)$,

$x_{24} = 0.33622\, (1 - \exp(-0.03442\, y))$,

$x_{25} = 0.0363\, \exp(-4.6\, x)\, (1 - \exp(- (z/38.7)^{4.97}))$,

$x_{26} = 1 + 2.751\, (1 - \exp(- (y/15.916)^{8}))$, $x_{27} = 60\, \Omega\, \ln(x_{30}/x + (1 + (2/x)^2)^{1/2})$,

$x_{28} = x_{27} / (x_{18})^{1/2}$, $x_{29} = x_{28}\, (x_{13}/x_{14})$^$(x_{17})$,

$x_{30} = 6 + (2\pi - 6)\, \exp(-(30.666/x)^{0.7528})$.

APPENDIX B

DEVICE PHOTOMASK

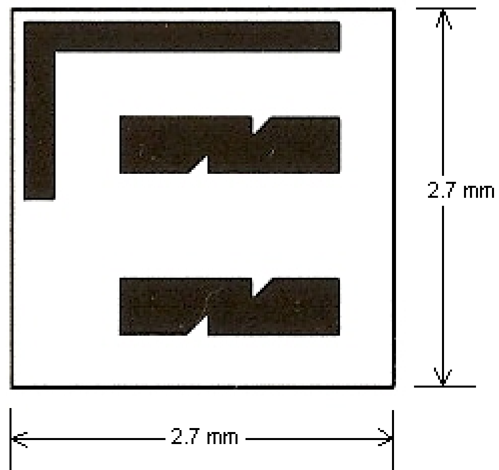

Black represents electrodes.

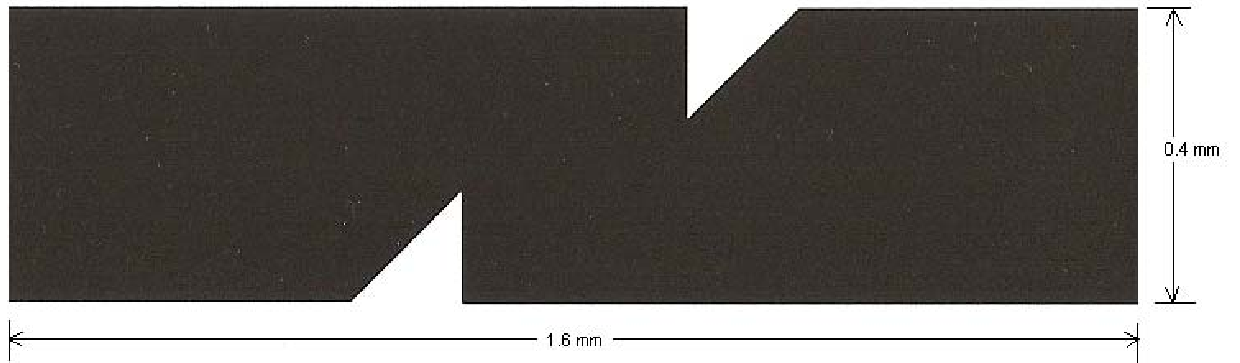

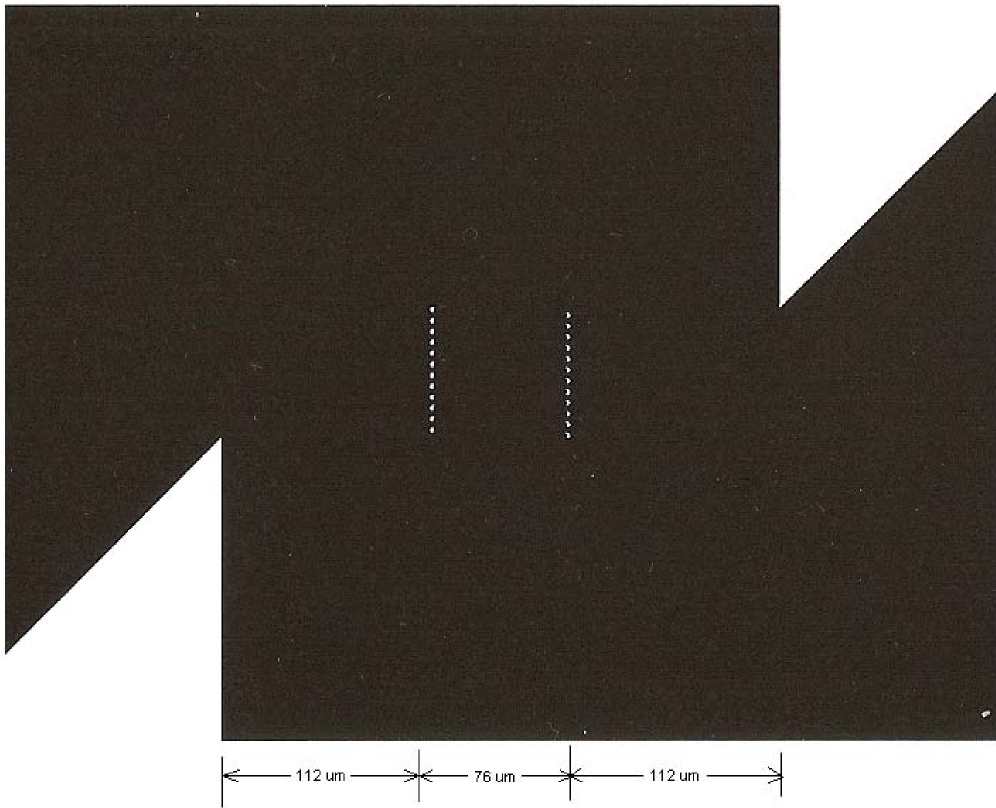

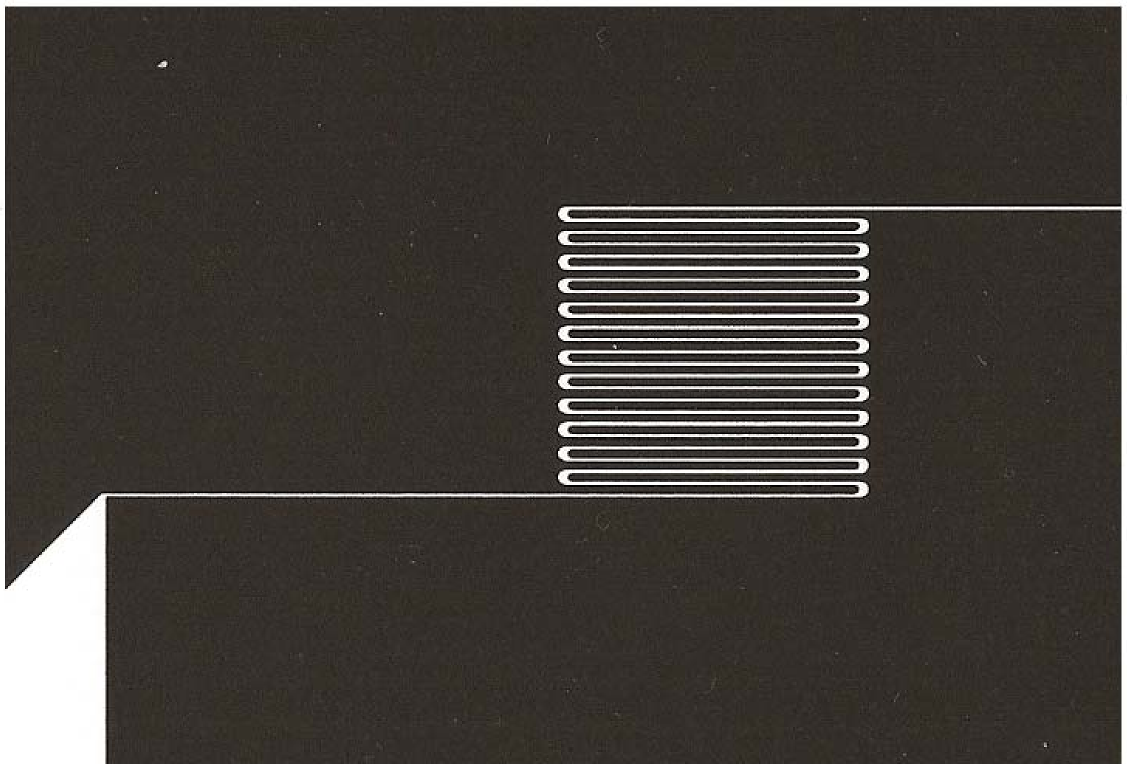

1.5 um electrode width and separation

REFERENCES

[1] Armin Karabegovic, “Photoswitch-Based Class E Microwave Power Amplifier”, PhD Dissertation, University of Missouri in Columbia, MO, 2007.

[2] Kelin J. Kuhn, “Laser Engineering”, Prentice-Hall, Inc., Upper Saddle River, NJ, 1998.

[3] Joseph T. Verdeyen, “Laser Electronics, 3rd Edition”, Prentice-Hall, Inc., Upper Saddle River, NJ, 1995.

[4] Stephen A. Campbell, “The Science and Engineering of Microelectronic Fabrication, 2nd Edition”, Oxford University Press, New York, NY, 2001.

[5] William C. Nunnally, “High-Power Microwave Generation Using Optically Activated Semiconductor Switches”, IEEE Transactions on Electronic Devices, Vol. 37, No. 12, December 1990.

[6] Donald A. Neamen, “Semiconductor Physics and Devices: Basic Principles, 2nd Edition”, McGraw-Hill, Chicago, IL, 1997.

[7] Sadao Adachi, “Properties of Group-IV, III-V and II-VI Semiconductors”, John Wiley and Sons Ltd., West Sussex, England, 2005.

[8] M. C. Beard, G. M. Turner, and C. A. Schmuttenmaer, “Subpicosecond Carrier Dynamics in Low-Temperature Grown GaAs as Measured by Time-Resolved Terahertz Spectroscopy”, Journal of Applied Physics, Vol. 90, No. 12, December 2001.

[9] S. Y. Chou and M. Y. Liu, “Nanoscale Tera-Hertz Metal-Semiconductor-Metal Photodetectors”, IEEE Journal of Quantum Electronics, Vol. 28, No. 10, October 1992.

[10] S. Averine, O. Bondarenko, and R. Sachot, “High-Speed Limitations of the Metal-Semiconductor-Metal Photodiode Structures with Submicron Gap Between the Interdigitated Contacts”, Solid-State Electronics, Vol. 46, pp. 2045-2051, 2002.

[11] S.-W. Seo, S.-Y. Cho, S. Huang, J. J. Shin, N. M. Jokerst, A. S. Brown, and M. A. Brooke, “High-Speed Large-Area Inverted InGaAs Thin-Film Metal-Semiconductor-Metal Photodetectors, IEEE Journal of Selected Topics in Quantum Electronics, Vol. 10, No. 4, July/August 2004.

[12] M. Mikulics, S. Wu, M. Marso, R. Adam, A. Forster, A. van der Hart, P. Kordos, H. Luth, and R. Sobolewski, "Ultrafast and Highly Sensitive Photodetectors With Recessed Electrodes Fabricated on Low-Temperature-Grown GaAs, IEEE Photonics Technology Letters, Vol. 18, No. 7, April 2006.

[13] W. C. Nunnally and R. B. Hammond, "Photoconductive Power Switches," Los Alamos Nat. Lab. Rep. LA-9759-MS, April 1983

[14] S. M. Sze, "Physics of Semiconductor Devices, 2nd Edition", John Wiley and Sons, Inc., New York, NY, 1981.

[15] Chih-Jung Huang, "Opto-electronic Class AB Microwave Power Amplifier Using Photoconductive Switch Technology", Master's Thesis, University of Missouri in Columbia, MO, 2006.

[16] Gunter Kompa, "Practical Microstrip Design and Applications", Artech House, Inc., Boston, MA, 2005.

[17] M. H. Eghlidi, K. Mehrany, and B. Rashidian, "Analytical Approach for Analysis of Nonuniform Lossy/Lossless Transmission Lines and Tapered Microstrips", IEEE Transactions on Microwave Theory and Techniques, Vol. 54, No. 12, December 2006.

[18] Aleksandar Marincic, "Huygens-Kirchhoff's Theory in Calculation of Elliptical Gaussian Beam Propagation through a Lens", Microwave Review, December 2002.

[19] A. J. Wilkinson and J. K. A. Everard, "Transmission-Line Load-Network Topology for Class-E Power Amplifiers", IEEE Transactions on Microwave Theory and Techniques, Vol. 49, No. 6, June 2001.

[20] F. H. Raab, "Idealized Operation of the Class E Tuned Power Amplifier", IEEE Transactions on Circuits and Systems, Vol. CAS-25, pp. 725-735, December 1977.

[21] Richard C. Dorf and James A. Svoboda, "Introduction to Electric Circuits, 4th Edition", John Wiley and Sons, Inc., New York, NY, 1999.